U.PORTO

FEUP FACULDADE DE ENGENHARIA
UNIVERSIDADE DO PORTO

M 2023

DEVELOPMENT OF BIPHASIC GRANULES USING THE NANOXIM PROCESS FOR BONE REGENERATION

CARLOTA PINTO PEREIRA

MASTER'S DEGREE DISSERTATION OF MATERIAL ENGINEERING PRESENTED
TO THE FACULTY OF ENGINEERING OF UNIVERSITY OF PORTO

SUPERVISORS at FEUP

José Domingos Santos

Maria Ascensão Lopes

SUPERVISOR at FLUIDINOVA, S.A

Catarina Coelho

July 2023

U.PORTO
FEUP FACULDADE DE ENGENHARIA
UNIVERSIDADE DO PORTO

CANDIDATE	Carlota Pinto Pereira		Code 201806605
TITTLE	Development of biphasic granules using the nanoxim process for bone regeneration		
DATE	_____de_____de_____		
PLACE	Faculdade de Engenharia da Universidade do Porto- Room_____ - __:__h		
JURY	President	José Carlos Fonseca	DEMM/FEUP
	Contestant	João Bebiano Costa	
	Supervisor	José Domingos Santos	DEMM/FEUP

Abstract

The use of biomaterials as bone substitutes has shown promise in the regeneration of damaged bone tissue. Among the most used biomaterials are calcium phosphates ceramics, such as hydroxyapatite (HAp) and ß-tricalcium phosphate (ß-TCP). These materials mimic the chemical composition of the inorganic bone matrix and promote the formation of new bone tissue. Biphasic calcium phosphates are bone substitutes that are a mixture of HAp and ß-TCP with varying ratios, which have lately gained great interest. The objective of this work was to develop HAp and biphasic granules through the FLUIDINOVA's production process. These materials were characterized to assess their structural, physicochemical, and mechanical properties.

In this work, the color of HAp granules changed from white to pink as the sintering temperature increased. ICP analysis revealed higher concentrations of iron than expected, which can form pink-colored oxide compounds at high temperatures. XPS analysis confirmed the presence of iron oxides, specifically ferrous oxide (FeO) and ferric oxide (Fe_2O_3), as potential causes for the color change.

Through SEM analysis it was possible to observe the bonding of the particles within the granules with increasing temperature, leading to a reduction in their porosity and subsequent densification. The XRD analysis showed that until 1300 °C the granules had high crystallinity since their characteristic peaks are very narrow. At 1300 °C the HAp undergoes a phase transformation to TTCP (tetracalcium phosphate), obtaining granules with 92.15% HAp and 7.85% of TTCP. From a mechanical standpoint, compression tests and Vickers hardness tests were performed. With increasing sintering temperature there was a significant increase in both compressive strength and hardness values, leading to the conclusion that increasing the sintering temperature significantly enhances the mechanical properties. However, the highly porous structure of the materials leads to lower compressive strength and Vickers hardness compared to dense HAp, however suitable for trabecular bone replacement (10-80 MPa).

Subsequently, granules consisting of 75% HAp and 25% ß-TCP were produced. XRD analysis revealed a phase transformation of ß-TCP to α-TCP, a highly resorbable phase, at 1300 °C. Mechanically, despite the lower compressive strength compared to HAp granules due to higher porosity, the biphasic granules remained adequate as a substitute for trabecular bone. The porosity promoted rapid bone ingrowth, facilitating integration with new bone tissue and enhancing the overall bone regeneration process.

In future work, further investigation is needed to explore the observed color change in more depth. Specifically, conducting sintering in an oxygen-free argon atmosphere could be explored to avoid the formation of Fe oxides and consequent color change of the granules.

Keywords: Hydroxyapatite, ß-tricalcium phosphate, α-tricalcium phosphate, Biphasic calcium phosphates, Bone Substitutes, Compressive Strength, Vickers Hardness.

Resumo

A utilização de biomateriais como substitutos ósseos tem-se mostrado promissora na regeneração de tecido ósseo danificado. Entre os biomateriais mais utilizados estão as cerâmicas de fosfatos de cálcio, como a hidroxiapatite (HAp) e o ß-fosfato tricálcico (ß-TCP). Estes materiais imitam a composição química da matriz óssea inorgânica e promovem a formação de novo tecido ósseo. Os fosfatos de cálcio bifásicos são substitutos ósseos que são uma mistura de HAp e ß-TCP com proporções variáveis, que ultimamente têm ganho grande interesse. O objetivo deste trabalho foi desenvolver grânulos de HAp e bifásicos através do processo de produção da FLUIDINOVA. Estes materiais foram caracterizados para avaliar suas propriedades estruturais, físico-químicas e mecânicas.

Neste trabalho, a cor dos grânulos de HAp mudou de branco para rosa com o aumento da temperatura de sinterização. A análise ICP revelou concentrações de Fe elevadas, que podem formar compostos de óxido cor-de-rosa a altas temperaturas. A análise XPS confirmou a presença de óxidos de ferro, especificamente óxido ferroso (FeO) e óxido férrico (Fe_2O_3), como causas potenciais da mudança de cor.

Através da análise SEM foi possível observar a união das partículas no interior dos grânulos com o aumento da temperatura, levando a uma redução da sua porosidade e consequente densificação. A análise XRD mostrou que até 1300 °C os grânulos tinham alta cristalinidade, uma vez que os seus picos característicos eram muito estreitos. A 1300 °C a HAp sofreu uma transformação de fase para TTCP (fosfato tetracálcico), obtendo-se grânulos com 92,15% de HAp e 7,85% de TTCP. Do ponto de vista mecânico, foram efetuados ensaios de compressão e ensaios de dureza Vickers. Com o aumento da temperatura de sinterização registou-se um aumento significativo destes valores, o que permite concluir que o aumento da temperatura de sinterização melhora significativamente as propriedades mecânicas. No entanto, a estrutura altamente porosa dos materiais conduz a uma menor resistência à compressão e dureza Vickers em comparação com a HAp densa, mas adequada para a substituição do osso trabecular (10-80 MPa).

De seguida, foram produzidos grânulos constituídos por 75% de HAp e 25% de ß-TCP. A análise XRD revelou uma transformação de fase do ß-TCP em α-TCP, uma fase altamente reabsorvível, a 1300 °C. Mecanicamente, apesar da menor resistência à compressão em comparação com os grânulos de HAp devido à maior porosidade, os grânulos bifásicos são possíveis de utilizar como substitutos do osso trabecular. A porosidade promove um rápido crescimento ósseo, facilitando a integração com o novo tecido ósseo e melhorando o processo global de regeneração óssea.

Em trabalhos futuros, é necessária uma investigação mais aprofundada para explorar a mudança de cor observada. Especificamente, poderia ser explorada a condução da sinterização numa atmosfera de árgon sem oxigénio para evitar a formação de óxidos de Fe e a consequente alteração da cor dos grânulos.

Acknowledgments

Com o passar destes 5 anos, não poderia deixar de agradecer a todas as pessoas que de alguma forma fizeram parte deste percurso.

Em primeiro lugar, não poderia deixar de agradecer ao professor e orientador José Domingos Santos por todo o apoio e disponibilidade demonstrados ao longo da elaboração da minha dissertação. Graças à sua preciosa ajuda em todos os pormenores, foi possível concluir com sucesso estes 6 meses de trabalho.

Um agradecimento especial a todos os professores do Departamento de Engenharia de Materiais que fizeram parte do meu percurso académico e que de alguma forma me ajudaram a crescer, não só a nível académico, mas também a nível pessoal e cívico. À Professora Maria Ascensão Lopes, o meu agradecimento por toda a disponibilidade e apoio nestes últimos meses.

À grande empresa que me acompanhou nesta jornada, FLUIDINOVA, tenho de agradecer o companheirismo e o bom ambiente demonstrado sempre que estive presente. À Doutora Catarina, a quem agradeci todos os dias, agradeço mil vezes mais por toda a disponibilidade para me ajudar em todos os momentos e situações. A todos, o meu muito obrigado.

Também um agradecimento especial ao Miguel Rodrigues, por me ter acompanhado e ajudado na realização desta dissertação.

Aos meus amigos, aos meus grandes amigos que fizeram destes os melhores 5 anos da minha vida. Faria e repetiria tudo por mais e mais anos convosco ao meu lado. Para sempre.

Finalmente, e porque os últimos são sempre os primeiros, à minha família. Aos meus pais por me terem dado a oportunidade de viver este tão lindo percurso, por toda a educação, paciência e apoio, e claro, pelo dinheiro que gastaram comigo. Ao meu irmão e à Inês, os meus maiores pilares durante estes 5 anos, um enorme obrigado por estarem presentes todos os dias para tudo. À mais nova, obrigada por seres quem és, e por acreditares sempre em mim.

Aos meus primos, tios e avós, aos que estão e aos que não estão fisicamente presentes, obrigado por nunca terem desistido de mim, obrigado por estarem presentes na minha vida e por fazerem de mim a pessoa que sou hoje.

Não é possível meter em palavras tudo aquilo que sinto, nem descrever tudo o que passei nestes últimos anos. Ainda assim, obrigado a todas as pessoas que se cruzaram no meu caminho e por terem feito destes anos os melhores anos da minha vida!

Table of Contents

Abstract i
Keywords i
Resumo ii
Acknowledgments iii
1. Introduction 1
1.1. Contextualization 1
1.2. Objectives 2
2. Literature Review 3
2.1. Bone: structure, development and bone biology 3
2.1.1. Composition: Bone Matrix 3
2.2. Bone Remodeling 5
2.3. Types of Cells 5
2.3.1. Undifferentiated mesenchymal cells 6
2.3.2. Osteoblasts 6
2.3.3. Osteocytes 7
2.3.4. Osteoclasts 7
2.4. Bone regeneration 7
2.5. Bone graft substitutes 8
2.5.1. Autografts 9
2.5.2. Allografts 9
2.5.3. Xenografts 9
2.5.4. Synthetics 10
2.5.4.1. Bioceramics 10
2.5.4.1.1. Hydroxyapatite (HAp) 11
2.5.4.1.2. Tricalcium Phosphate (TCP) 11
2.5.4.1.3. HAp and β-TCP biphasic bioceramics 12
2.6. Bone grafts and substitutes: Market analysis 13
3. Methodology 16
3.1. Materials 16

3.1.1. FLUIDINOVA's Hydroxyapatitite 17
3.1.2. FLUIDINOVA's β-TCP 17
3.1.3. Sample's Preparation 18
3.2. Experimental Procedure 19
3.2.1. Slurry Preparation 19
3.2.2. Slurry extrusion 20
3.2.3. Crosslinking 21
3.2.4. Washing 21
3.2.5. Drying 21
3.2.6. Sintering 21
3.2.7. Sieving 22
3.3. Granules Characterization 22
3.3.1. Scanning Electronic Microscopy 22
3.3.2. X-Ray Diffraction 22
3.3.3. Linear and Volume Shrinkage 23
3.3.4. Bulk density 23
3.3.5. Inductively Coupled Plasma – Atomic Emission Spectrometry (ICP- AES) 24
3.3.6. X-Ray Photoelectron Spectroscopy (XPS) 24
3.4. Mechanical Characterization 25
3.4.1. Compression Tests 25
3.4.2. Vickers Hardness Tests 26
3.5. Statistical analysis 26
4. Results and Discussion 27
4.1. Granules Characterization 27
4.1.1. Monophasic Granules 27
4.1.1.1. Granules color 27
4.1.1.2. Scanning Electronic Microscopy 28
4.1.1.3. X-Ray Diffraction 31
4.1.1.4. Linear and Volume Shrinkage 33
4.1.1.5. Bulk Density 34
4.1.1.6. Inductively Coupled Plasma – Atomic Emission Spectrometry (ICP- AES) 35
4.1.1.7. X-Ray Photoelectron Spectroscopy (XPS) 36

4.1.2. Biphasic Granules 38
4.1.2.1. Bulk Density 38
4.1.2.2. X-Ray Diffraction 39
4.2. Mechanical Characterization 41
4.2.1. Monophasic Granules 41
4.2.1.1. Compressive tests 41
4.2.1.2. Vickers hardness tests 43
4.2.2. Biphasic Granules 45
4.2.2.1. Compressive tests 45
5. Conclusions and Future work 47
6. References 48
Appendix I 53

List of Figures

Figure 1- Representative model of trabecular and cortical bone [8]. 4

Figure 2- Schematic representation of the bone remodeling process [45]. 5

Figure 3- Representation of the types of cells that are present in a bone [8]. 6

Figure 4- Four main types of bone graft substitutes: a) granule; b) block; c) cement; d) putty [18, 46]. 13

Figure 5- Growth rate by region- Bone graft and substitutes market [34]. 14

Figure 6- United States bone graft and substitutes market, growth rate by material type (2020-2030) [35]. 15

Figure 7- Flow chart of the production process for nanoXIM granules [40]. 19

Figure 8- Slurry preparation using a mechanical stirrer. 20

Figure 9- Spheres' production method. A) nanoXIM•G1000 granules' encapsulator; B) nanoXIM•G2000 granules' encapsulator. 20

Figure 10- Spheres' formation into the calcium chloride solution. 21

Figure 11- Equipment used for the mechanical tapping to calculate the bulk density. . 24

Figure 12- Equipment, Compact Tabel-Top Universal / Tensile Tester from Shimadzu, used in this work. 25

Figure 13- Color change of HAp granules from white to pink color when increasing the sintering temperature. 27

Figure 14-A) Macroscopic view of the HAp granules; B) Spherical shape of the granules; Images obtained through SEM relative to C) Before sintering and D) HAp1300 (after sintering), that provide a perspective of the granules, clearly displaying their spherical shape and size. 28

Figure 15- SEM images reveal the surface characteristics of non-sintered HAp spherical granules and sintered at temperatures of 1200 and 1300 °C. 29

Figure 16- SEM images with the measurements of pores sizes on the samples: A) non-sintered and B) HAp1300. 30

Figure 17- SEM images of A) HAp1000 and B) HAp1300. 31

Figure 18- Diffractogram obtained through X-Ray diffraction analysis of HAp1000. 31

Figure 19- Weight fraction of existing phases in HAp1300. 32

Figure 20- Diffractogram obtained through X-Ray diffraction analysis of HAp1300. 32

Figure 21- Granules' volume evolution with sintering temperature of each batch. 33

Figure 22-Granules' average volume evolution with average porosity of each batch. ... 33

Figure 23- XPS global spectrum of HAp1200, being representative of all samples. 37

Figure 24- Fe's XPS spectrum for A) Bp1200 and B) Bp1300. 37

Figure 25- Diffractogram obtained through X-Ray diffraction analysis of all biphasic batches. 40

Figure 26- Diffractogram obtained through X-Ray diffraction analysis of Bp1000 and Bp1300. 40

Figure 27- Compressive strength results obtained for each batch. 43

Figure 28- Vickers hardness of the samples as a function of their porosity. 44

Figure 29- Indentations of Vickers hardness tests on: A) HAp1000 and B) HAp1300. 45

Figure 30- Compressive strength obtained values for each batch..... 46

List of Tables

Table 1- Main specifications of FLUIDINOVA's HAp granules. Adapted from [37]. 16

Table 2- Main properties of FLUIDINOVA's HAp granules. Adapted from [37]. 16

Table 3- Properties of FLUIDINOVA's nanoXIM•HAp202 HAp. Adapted from [38]. 17

Table 4- Properties of FLUIDINOVA's nanoXIM•TCP600 B-TCP. Adapted from [39]. 17

Table 5- Designation of each batch of HAp granules produced and the sintering temperatures used. 18

Table 6- Designation of each batch of biphasic granules produced and its composition. 18

Table 7- Relative density values obtained for each batch, along with their corresponding global porosity. 34

Table 8- Elements concentration (ppm) after ICP analysis. 35

Table 9- Relative density values obtained for each batch, along with their corresponding global porosity. 39

Table 10- Batches' phase quantification obtained through XRD. 41

Table 11- Compressive strength's average values for each batch. 42

Table 12- Average hardness values of each sample. 44

Table 13- Compressive strength's average values for each batch. 45

Table 14- ICP analysis' results of the raw materials, the HAp powder and the granules produced. 53

Abbreviations list

HAp - Hydroxyapatite

ß-TCP - ß-Tricalcium phosphate

BCPs - Biphasic calcium phosphates

BMU - Basic multicellular unit

BLCs - Bone lining cells

MSCs - Mesenchymal stem cells

CaO - Calcium Oxide

SEM - Scanning Electronic Microscopy

XRD - X-Ray Diffraction

XPS- X-ray Photoelectron Spectroscopy

ICP-AES- Inductively Coupled Plasma – Atomic Emission Spectrometry

1. Introduction

1.1. Contextualization

The aging population highlights the urgent need for improved therapies to address bone diseases and injuries. In recent years, the use of bioactive and biodegradable materials with temporary structural functions to aid in bone tissue regeneration has shown great promise. Calcium phosphates, a synthetic biomaterial used as bone substitutes, has been developed and offers distinct advantages, which make them highly appealing compared to other types of bone substitutes. Their choice varies based on the nature and severity of the injury, including autologous, allogenic, xenogenic, or synthetic options. Although autologous bone substitutes are commonly used, there is a growing demand for synthetic bone substitutes. Calcium phosphates can mimic the chemical composition of the inorganic bone matrix. Their biocompatibility and bioactivity stimulate bone cell growth at the implantation sites, leading to reduced post-surgery recovery times [1, 2].

Initial efforts in the synthesis and design of calcium phosphate (CaP) bone graft substitutes primarily focused on sintered forms of hydroxyapatite (HAp), tricalcium phosphate (β-TCP), or their combinations. The objective was to create a material resorbable enough to undergo complete conversion into bone during the process of bone regeneration. HAp was chosen for its resemblance to bone mineral in terms of crystallographic structure and composition, as well as its high compressive strength and relatively simple production process. However, unlike bone mineral that can undergo remodeling through the activity of osteoclasts, sintered HAp requires a extend period for its absorption and assimilation into the bone site. On the other hand, β-TCP, although less stable, demonstrates greater bioactivity. This characteristic allows for the material to be gradually broken down and absorbed by the body as new bone forms during the regeneration process [3–5].

To overcome these limitations, and as the main theme of this dissertation, the production of biphasic granules comprising both HAp and β-TCP has emerged as a highly relevant and promising area of research in the field of bone regeneration. This combination harnesses the synergistic properties of each phase, capitalizing on their respective advantages to enhance the efficiency of bone regeneration. By varying the ratio of the phases that make up the granules, it is possible to create a more biodegradable material or a material with superior mechanical properties, which makes them appealing for bone regeneration applications [3–5].

Besides this brief theoretical introduction to the subject, it is important to highlight that this dissertation was developed in partnership with FLUIDINOVA, S.A., a company specialized in the manufacture of synthetic calcium phosphate materials for medical devices, oral and food industries.

1.2. Objectives

The objective of this work is to develop monophasic hydroxyapatite granules, study and evaluate their physicochemical and mechanical properties with different sintering temperatures. Then, biphasic granules for application in the field of bone regeneration were produced, employing FLUIDINOVA's proprietary production methodology. These granules consist of two distinct phases: hydroxyapatite and ß-tricalcium phosphate.

Following that, the emphasis will be on evaluating the influence of the sintering temperature on the ultimate properties of the biphasic granules, specifically their structural and mechanical properties, with the goal of determining how the addition of the ß-TCP phase influenced the overall properties of the granules and whether they exhibited advantages in terms of their potential applications for bone regeneration.

The final goal of this work is to contribute to the development of an innovative and new product for the company. The introduction of this product will not only expand the company's medical device portfolio, but will also open new market opportunity, as FLUIDINOVA currently just markets pure hydroxyapatite spherical granules.

2. Literature Review

2.1. Bone: structure, development and bone biology

Bone forms the skeleton which serves as an internal structural support system for vertebrates. It has crucial functions in the body such as facilitating movements, harboring bone marrow and support and protection of soft tissues such as the brain. Despite that, bone has metabolic functions including secretion of hormones that regulate both mineral and energy metabolism. It is a mineralized connective tissue, natural and porous that participates in the body's calcium/phosphate balance. To maintain the amounts required to support physiological activities, these minerals that have been integrated into bone tissue can be released back into the bloodstream [6–8].

Bone has other essential functions such as fat storage and blood cell production. The interior of most bones has a rich vascular supply, with areas containing red bone marrow where the production of blood cells takes place. It is composed of osteoblasts, bone lining cells, osteocytes, and osteoclasts, which make it a highly dynamic organ. There are two important processes that occur throughout the life of the bone, which need to occur simultaneously to be effective: growth and remodeling. Firstly, it is continuously formed, increased in size and shape, and remodeled, where the bone is continuous renewal of the skeleton by remodeling [6–8].

Besides that, bones can be classified according to their shape as: long (femur and tibia), short (carpals and tarsals), flat (sternum, ribs and cranial bones), irregular (facial bones and vertebrae) and sesamoid bones (patellae). According to their shape, they have different functions such as movement, support and stability for long and short bones; as points of attachment for muscles and protects internal organs for flat bones; to protect internal organs, movement and support by irregular bones and finally to protect tendons from high forces and allow muscle action by sesamoid bones [6–8].

2.1.1. Composition: Bone Matrix

Bone can be divided into cortical and trabecular, where 80% of the bone mass is in the cortical part (figure 1). They differ from each other in their function and morphology and depending on the type of bone that is selected, the ratio between these two structures may vary. This architecture offers a higher mechanical resistance and allows bone to deform significantly before failing. The cortical bone is a compact, dense hard and calcified part that surrounds the marrow cavity with hematopoietic elements, fat and spicules of bone. It also contains Haversian and Volkmann's canal systems for vascular supply, with a lamellar structure [9].

Cortical bone can be made of woven (primary) or lamellar (secondary) bone. The embryonic skeleton is made of woven bone, which is then resorbed and replaced by mature bone as the skeleton grows. After the age of approximately five years, woven bone doesn't make up the human skeleton, except for small parts of tendons and ligament

attachments, the suture margins of the cranial bones, and the ossicles of the ear. They differ to lamellar bone because of their formation, composition, organization, and mechanical properties [9].

For another hand, the trabecular bone is a highly porous and structurally anisotropic, with lower density and elasticity. Despite this porosity, it is composed of thin spicules and trabeculae of bone, separated by marrow spaces and blood vessels which increase the blood cell production. Compared to the cortical bone, the trabecular one is more metabolic active [7, 10, 11].

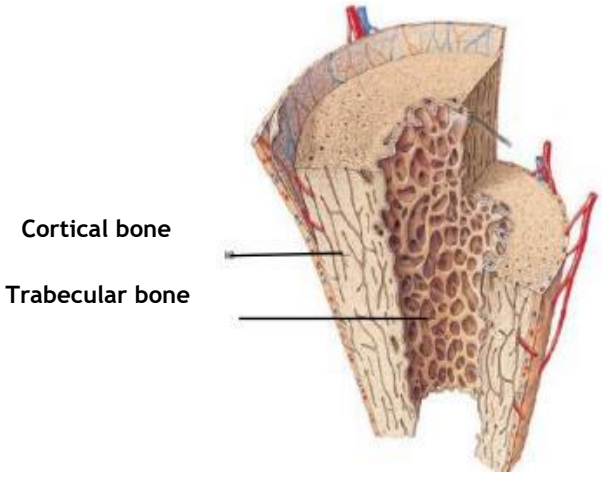

Figure 1- Representative model of trabecular and cortical bone [8].

The bone matrix is a composite material, made of organic and inorganic components, where the inorganic part makes up approximately 65% of the weight of the bone, the organic component accounts for about 25% and the remaining 10% is water. The organic part has similar characteristics to the matrix of dense fibrous tissues, such as tendons and ligaments. It is largely composed of type I collagen and has non-collagenous glycoproteins and bone-specific proteoglycans. Type I collagen is the most common type of collagen found in most connective tissues, which differs from other collagens in its biochemical structure. It is a fibrillar type collagen with a structure composed of a repeating tripeptide sequence that formed a triple-helical molecule, that offers an adhesion-promoting scaffolding surface for inorganic salt crystals [6, 8, 9].

The non-collagenous proteins, such as osteonectin and osteocalcin, blood proteins, and growth factors, form the other part of the organic matrix, which influence the mineralization of the bone and the bone cells's behavior. The inorganic matrix gives bone most of its stiffness and strength and its main component is calcium HAp $Ca_{10}(PO_4)_6(OH)_2$. These salt crystals result from the nucleation and recrystallization of calcium phosphate ions present in the matrix and are dispersed throughout the bone, arranged parallel to collagen fibers. While collagen fibers provide a framework for calcification and provide the bone flexibility so that it can bend without becoming brittle, HAp crystals give bones their hardness and strength [6, 8, 9].

2.2. Bone Remodeling

Bone remodeling is an overly complex process where old bone is replaced by new bone to keep its stability and integrity, to adapt to mechanical load and strain. On the other hand, a balance of bone resorption and formation is particularly important to avoid bone diseases like osteoporosis. For instance, excessive bone loss (osteoporosis) is caused by osteoclast activity without an equal quantity of bone being created by osteoblasts, whereas the opposite may lead to osteopetrosis, an increase in bone mass [6, 12].

Bone remodeling contains three consecutive phases (figure 2): resorption, reversal, and formation, with different duration times (from about two weeks to four months). Firstly, osteoclasts begin to resorb bone, which is followed by the transition from resorption to production of new bone (also known as the reversal period), where mononuclear cells appear on the bone surface. Finally, these cells interfere with osteoblasts, providing signals to the formation of new bone and its differentiation and migration. Also, osteocytes and bone lining cells interfere in this process, and together form a basic multicellular unit (BMU). After that, there is a prolonged period of rest before a new remodeling cycle starts [6, 12].

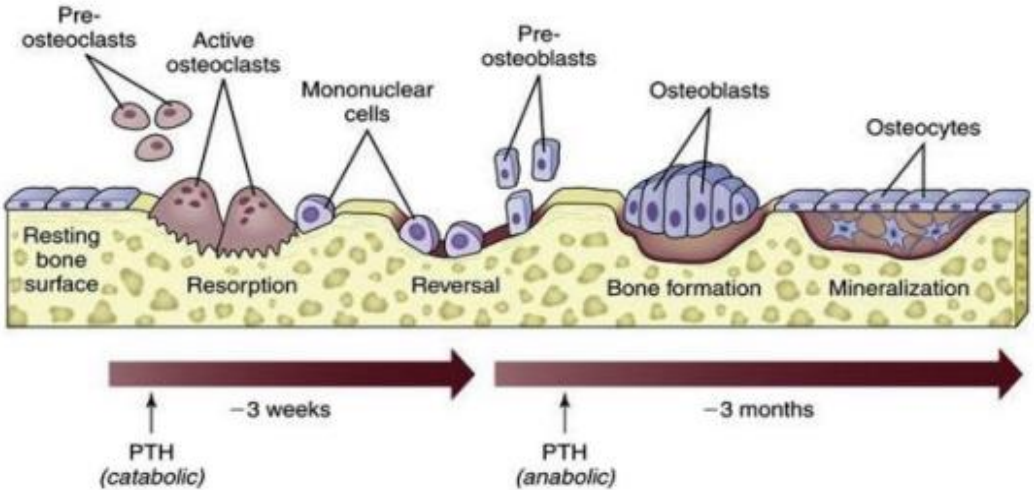

Figure 2- Schematic representation of the bone remodeling process [45].

2.3. Types of Cells

Bone cells make up less than 2% of the bone mass but have crucial functions. They differ from each other by morphology, function and characteristic locations and are responsible from the formation of bone to its resorption. Osteoblasts, osteoclasts, osteocytes, and osteogenic cells are the most important cells that are present in bone's cellular activity (figure 3) [13].

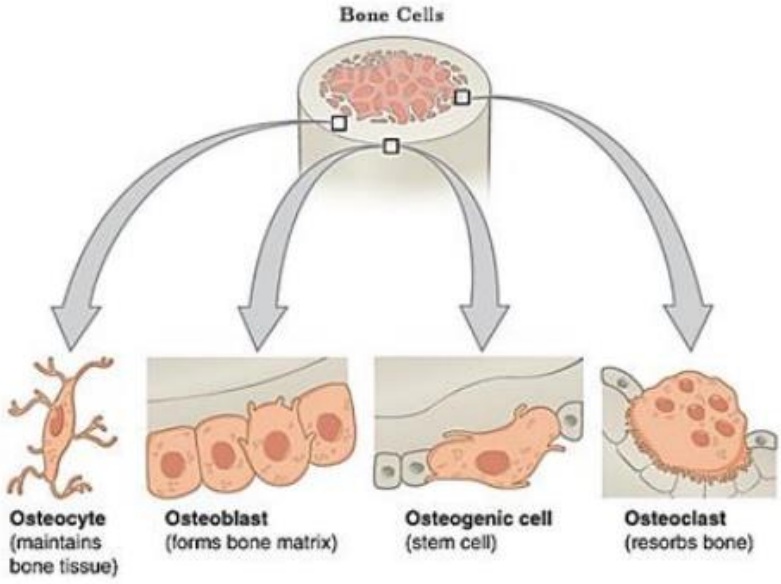

Figure 3- Representation of the types of cells that are present in a bone [8].

2.3.1. Undifferentiated mesenchymal cells

Undifferentiated mesenchymal cells have the capacity to proliferate and differentiate in other cells, such as osteoblasts, chondroblasts, bone marrow stromal cells, fibroblasts, muscle cells or adipocytes depending on their natural stimulation. They have an irregular form, one nucleus and a few organelles until their migration, proliferation, and differentiation, and can be found at bone canals and marrow, for example [7, 9].

2.3.2. Osteoblasts

Osteoblasts make up 4-6% of the total resident bone cells and have the known function of forming bone. They derive from mesenchymal stem cells with the ability to multiply differentiate into several connective tissue cell types based on the different stimulus present in their immediate environment, as mentioned before. With the correct stimuli to differentiate into osteogenic lineage, firstly they form osteoprogenitor cells, that still have the capacity of proliferating. The inner layer of the periosteum, the endosteum lining marrow cavities, osteonal (Haversian) canals, perforating (Volkmann's) canals, and perivascular tissue next to bone are all places where osteoprogenitor cells can be found [6, 7, 14].

The characteristics and developmental phases of mature osteoblast cells affect their shape, phenotype, and biosynthetic activity. Active osteoblasts are rounded, mononuclear, cuboidal cells that are resting on the matrix that they have created in aggregates, such as during bone development or fracture repair. Firstly, osteoblasts have the responsibility of proteoglycans and type I collagen’s production and deposition, that mostly make up the osteoid, the organic part of bone matrix. Then, occur osteoid mineralization, through the release of matrix vesicles and the deposition of calcium and

phosphate [6, 7, 14].

2.3.3. Osteocytes

Osteocytes compromise 90-95% of all bone cells, with the highest abundance and the longest longevity, with a lifespan of up to 25 years. They derive from osteoblasts which have become trapped within the bone matrix produced by themselves. The osteocytes have a dendritic shape and are found in lacunae surrounded by mineralized bone matrix, usually in cortical and trabecular bone tissue. The contact between osteocytes within the bone matrix and cells outside is made possible through long intercellular processes like cytoplasmic processes that form a complex and vast cell network. Additionally, it is known that osteocytes are cells that respond to mechanical loading and oversee activating cellular processes (such as bone production and/or remodeling) by transferring load. For example, when the skeleton is under mechanical stress, osteocytes sense pressure changes in bone, that result in chemical instructions being transmitted to the surface cells to respond by either forming or resorbing bone [6, 7, 14].

2.3.4. Osteoclasts

Osteoclasts are multinucleate cells (3-25 nuclei per cell) responsible for bone resorption or breakdown and are derived from two types of white blood cells: monocytes and macrophages. It is important to have colony stimulating factors for the proliferation and differentiation of osteoclast progenitor cells, but only with other cytokines occur their activation and bone resorption. Their main functional capacity is based on pump acid into specific resorption pits to dissolve bone mineral and to create the ideal conditions for the enzymatic breakdown of demineralized extracellular bone matrix. Thus, they are primarily found in places where resorption is occurring or has already occurred, such as pits or cavities [7, 14].

2.4. Bone regeneration

Bone regeneration, which may be observed in response to typical fracture healing, is involved in continual remodeling throughout adult and during skeletal growth, is a complex physiological process of bone creation [15].

The bone development or ossification only begins by the sixth or seventh week of embryonic life in utero and persists through adolescence. Before that the embryo’s skeleton is based on fibrous membranes and cartilage. Two mechanisms (which are distinct from each other on the pathway to produce new bone) are responsible for the actual development of the bone. But regardless of the mechanism that created it, mature bone is the same [16].

Firstly, intramembranous ossification is a fast process that results in a compact and spongy bone, where mesenchymal cells in the embryonic skeleton can directly start

to multiply and differentiate into specialized cells at this point. Some of them develop into osteogenic cells, which later become osteoblasts. Then, the osteoblasts developed will thereafter congregate in the ossification center, that around the capillaries to form the trabecular matrix of the bone. This process is the principal former of craniofacial skeleton [8, 17].

Secondly, the endochondral ossification is a much longer process where the mesenchymal cells can differentiate into cartilage cells (chondroblasts) that serves as a template to be totally replaced by new bone. Cartilage is a flexible, semi solid matrix made of water hyaluronic acid, chondroitin sulfate and collagen fibers. Contrary to most connective tissues, cartilage lacks blood arteries that would transport nutrients and metabolic waste away, which is achieved by diffusion from vessels in the perichondrium, a membrane that surrounds the cartilage. This process occurs in two distinct locations: diaphyseal and epiphyseal, respectively, the primary and secondary sites of ossification. Osteoblasts brought by blood vessels in the perichondrium arrive and deposit bone in a ring around the diaphysis (bone collar), that prevent nutrients from reaching to the center of hyaline cartilage. So, death and disintegration of chondrocytes will occur in the center of the structure. Without cartilage, blood vessels enter the resulting spaces, increasing the cavities and bringing osteogenic cells with them—many of which will develop into osteoblasts—that in turn cause the spaces to widen and form the medullary cavity. Bone is now deposited, and the primary ossification center is established. The secondary site of ossification only takes place after birth, where the same sequence of events occurs in the epiphyseal regions. Endochondral ossification is the process by which most of the skeleton is formed, like skull and long bones [8, 17].

2.5. Bone graft substitutes

Bone can regenerate under certain conditions like it is mentioned before. However, this ability is confined to minor bone defects. Large-scale bone healing is not biologically possible, such as defects caused by open injury or through the removal of tumors. In these cases, is necessary to have a surgical intervention, where are used materials serving as a bridge to maintain and, ideally, accelerate bone formation, a mechanism known as bone grafting. After blood transfusions, bone is the tissue transplant performed most frequently around the world, because of the advantages in terms of cost, speed, versatility, increased safety profiles, and ease of use and handling. A bone substitute must have some important properties namely biocompatibility and do not provoke any adverse inflammatory response; should be resorbable, osteoinductive and osteoconductive; quickly set and easily molded into the bone defect; thermally nonconductive and sterilizable [18, 19].

Bone grafting is a process based on sequence steps: firstly, a buildup of inflammatory cells and the chemotaxis of host mesenchymal cells to the graft site provoked by the placement of the bone graft. Then, under the influence of numerous osteoinductive stimuli, the primitive host cells develop into osteoblasts. Additionally,

necrotic graft degradation and bone graft revascularization take place simultaneously. Finally, osteoblasts attach to the three-dimensional framework of the graft and produce bone, followed by bone remodeling in response to mechanical stress [13, 18, 19].

On a medical point of view, bone substitutes can be divided into natural (autografts, xenografts and allografts) and synthetic, according to their origin [20].

2.5.1. Autografts

Autografts are the "gold standard" of bone grafts for promoting bone growth. Autologous or autogenous bone grafting consists of using patient's own bone as a graft. So, non-essential bones like the iliac crest, fibula, chin, ribs, mandible, and even portions of the skull can be used to harvest bone. These bones have the essential properties for bone regeneration, mainly osteoconductive and osteoinductive, and carry no danger of infection or immunological compromise. However, the autografts have some disadvantages related to a lengthier surgical time; the need of a surgical donor site, which could result in post-operative discomfort and problems, and some supply limitations related to how much bone tissue can be harvested, since it is not possible to harvest a high-volume fraction of bone [13, 18].

2.5.2. Allografts

Allografts are an alternative to autografts, where the main difference is whether the replacement bone comes from living (for example, patients that had a total hip replacement surgery) or nonliving/cadaver donors. Therefore, allografts can be kept in a bone tissue bank and used to treat a greater number of patients because the supply is virtually limitless. However, there have been some reported storage-related issues. On the other hand, allografts can be manipulated to achieve a specific shape or texture, such as creating a cortical ring for spinal fusion. In the US, demineralized bone is a commonly used substitute for bone grafts and is typically utilized as a moldable paste [13, 18, 21].

They have the main properties to replace bone, osteoconductive and weakly osteoinductive, but they also come with some risks, such as the possibility that a disease will be transmitted from donor to recipient and may trigger immunogenic reactions. For this reason, this type of bone graft substitute is usually defusing of proteins normally found in healthy bone and submitted to a sterilization process, with gamma irradiation, for one hand to prevent the loss of some mechanical properties but it causes the loss of some their biologic properties. So, preparing allografts that are thoroughly clean, sterile, and virus-free while maintaining the tissue's original biochemical and biomechanical qualities is difficult [13, 15, 16, 18].

2.5.3. Xenografts

Unlike the two types of grafts mentioned above, xenografts are a type of transplant where bones from one species (the donor) are implanted or grafted into a

different species (the recipient), in this case they come from non-human bone, such as bovine or porcine bone, and have properties that make them biocompatible with human recipients and conducive to bone growth. Bovine-derived xenografts are processed to remove the organic component and retain the natural bone mineral structure, so they are usually freeze-dried or demineralized and deproteinized. However, they can carry a theoretical risk of disease transmission, rejection and have failed in the past due to residual proteins left behind after processing. Although the analysis of available data suggests that the risk associated with using these bone grafts is low, there are still significant concerns. The fragile and brittle nature of xenogenic bones means that a more delicate surgical approach is necessary, as they tend to break during the fixation process. This may also impact the healing process [18, 22].

2.5.4. Synthetics

2.5.4.1. Bioceramics

Bioceramics are a class of ceramic materials used for reconstruction and regeneration of hard tissues (musculoskeletal systems), that have been receiving a lot of attention and growing usage in clinical applications such as for synthetic implants and prostheses. However, bioceramics have low mechanical resistance compared to metals, some difficulties of manipulation during surgical operations and very low ductility. Utilizing metallic implantations with bioceramic coatings, that combines the better properties of these two classes of materials, is one way to get around these challenges [20, 23, 24].

Bioceramics can be classified in three different types: bioinert (alumina and zirconia), bioactive (e.g., bioactive glass) and bioresorbable ceramics (e.g. porous ß- and α-tricalcium phosphates (TCP)) based on the response caused in the human organism when in contact with the host bone [20, 23, 24].

Bioinert ceramics cause minimal or no tissue response and are not resorbable. Because of that they can't interfere with the process of bone regeneration, so they are not usually used as scaffolds. They are mainly used as acetabular cups and femoral heads for hip replacement and for dental implants. Zirconium oxide (zirconia) and aluminum oxide (alumina) are examples of bioinert ceramics [20, 24, 25].

Bioactive ceramics, a class between bioinert and bioresorbable ceramics, stimulate the attachment of neighboring tissue with, for example, stimulation of new bone growth, which is the primary requirement in the selection of bioceramics to make scaffolds. In this class, there are materials such as bio-glass and HAp [20, 24, 25].

Bioresorbable or degradable ceramics are incorporated into the surrounding tissue or may even be completely dissolved over time. At the same time, the normal bone host tissue gradually takes their place which takes a challenging combination and optimization of the rate of tissue regeneration and resorption, as well as the subsequent

loss of mechanical qualities. Despite that, it brings the advantage of not having to remove the material later, in a second surgery. Here we can include, for example, porous tricalcium phosphate, $Ca_3(PO_4)_2$, in its α and ß phases [24, 25].

2.5.4.1.1. Hydroxyapatite (HAp)

HAp, $Ca_{10}(PO_4)_6(OH)_2$, is a naturally occurring mineral form of calcium apatite that makes up the main structural component of bones, around 70% of bones, and teeth in vertebrates. In natural HAp, the Ca/P ratio is approximately 1.67, which means there are 1.67 calcium ions for every phosphate ion in the crystal structure. Also, HAp is classified as a non-stoichiometric apatite because it may contain CO_3, Mg, Na, F, or Cl in its molecular structure. The existence of these molecules or elements lowers the Ca/P ratio of the HAp, leading to a reduction in the component's stability. Furthermore, the Ca/P ratio can also vary in synthetic HAp, depending on the method of synthesis and processing conditions. For biomedical applications, it is often desirable to have a Ca/P ratio that is like that of natural HAp to ensure good biocompatibility and integration with living tissue [18, 23, 25].

Since the human bone's mineral composition is mainly nanocrystals of HAp and due to the striking resemblance from synthetic HAp to the inorganic mineral component of bone, it is widely used in a variety of biomedical applications such as in the repair of bone defects as bone grafts. Synthetic HAp is an illustration of a bioactive ceramic, a manufactured version of the naturally occurring mineral form of calcium apatite. Despite that, based on crystallographic and chemical research, HAp is recognized to be identical to naturally occurring HAp, but is produced through chemical synthesis in a laboratory setting. HAp can be engineered to have specific characteristics, such as varying porosity, surface area, and particle size, making it a versatile biomaterial for a wide range of applications [18, 26–28].

Despite its remarkable biological characteristics, HAp has limited mechanical properties, particularly low fracture toughness. Another significant issue with HAp is the extended period required for its absorption and assimilation into the bone site. During this prolonged period where neither remodeling or new bone formation occurs, HAp's strength may deteriorate, resulting in implant fragility. As a result, biphasic composites were created to mitigate the associated risks and drawbacks, resulting in a material with better mechanical resistance and a higher degree of resorption, being a benefit in many applications. Typically, HAp is blended with tricalcium phosphate (TCP) to produce a biphasic ceramic [28–30].

2.5.4.1.2. Tricalcium Phosphate (TCP)

Tricalcium Phosphate is a bioceramic material that is commonly used in biomedical applications, particularly in orthopedic and dental procedures. It is a calcium phosphate compound with the chemical formula $Ca_3(PO_4)_2$, and it is biocompatible, bioresorbable, osteoinductive and osteoconductive, meaning that it supports the

formation of new bone tissue. TCP has a ratio Ca/P of 1.5, containing about 39% calcium and 20% phosphorus, and can be classified into two phases, namely α-phase and β-phase, depending on stability temperatures. The crystal structure of α-TCP is monoclinic, while β-TCP has a rhombohedral crystal structure. β-TCP has higher solubility and faster degradation rates, leading to increased biocompatibility.

Furthermore, β-TCP supports the growth of osteoprecursor cells such as osteoblasts and bone marrow stromal cells, and for this reason is usually chosen for bone regeneration applications, and an excellent choice for improving the biocompatibility of bone grafts. This is largely due to its structure, which enables optimal biomineralization and cell adhesion as supported by sources. However, the high resorption rate of β-TCP compared to HAp can be a cause for concern. This is one of the reasons why HAp is preferred in many biomedical applications, since when the resorption rate is higher than the rate of bone tissue formation, it can lead to implant instability and the growth of fibrous tissue that can occupy the spaces meant for bone growth [29, 30, 33, 34].

2.5.4.1.3. HAp and β-TCP biphasic bioceramics

As previously mentioned, research has been conducted over time to address the limitations of HAp and β-TCP in biomedical applications, with the goal of improving their performance. Therefore, scientists have explored the use of a combination of these two bioceramics to create a biphasic ceramic, which has been investigated and utilized in the field of biomedicine.

Biphasic calcium phosphate (BCP) is a composite material composed of two different calcium phosphate phases, typically HAp, more stable and β-TCP, more soluble, that are combined in varying proportions. The unique combination of HAp and β-TCP in BCP provides it with advantageous properties compared to monophasic calcium phosphate ceramics, such as improved biocompatibility, osteoconductivity, and bioresorbability. The different phases also allow for a controlled release of calcium and phosphate ions, which can enhance bone growth and regeneration. During granules' processing, sintering is a crucial step that consolidates the shaped forms, where several processes occur, such as the removal of humidity, carbonates, and other volatile chemicals from synthesis. This leads to shrinkage and densification of the powders, as well as an increase in grain size [3, 4, 33].

The success of bone graft substitute materials in the commercial market depends greatly on their handling characteristics. Most bone graft substitutes are typically used as granules that have a diameter of 0.1 to 5 mm or as porous blocks (pre-forms), due to the significance of having pores in a size range that facilitates quick bone growth into the material. Nonetheless, these bone graft substitutes that are highly porous cannot be utilized for orthopedic applications that undergo mechanical stress since the mechanical strength is negatively impacted by porosity. Contrarily, granules can fill any type of defect, but their handling is poor. Specifically, it is challenging to fill narrow defects with granules, and if any of the granule's spill outside the border of the defect, they must be

removed, which can be a tedious task. Using granules that are appropriately sized to match the defect size can make the application process neater [5, 21].

So, there are also formulations that harden after being implanted or injected in situ, such as calcium phosphate (CaP) cements. The ability to inject a CaP hydraulic cement (an injectable paste) expands their use, particularly for minimally invasive techniques for bone fracture treatment. However, this method is expensive, and the process of mixing CaP cement still involves a significant number of manual tasks before injection can occur. Moreover, once the CaP cement is mixed, there is only a restricted amount of time available for it to be injected [5, 21].

In addition to granules, porous blocks, and hardening paste, non-hardening pastes are also proposed, which are typically a mixture of granules and a highly viscous hydrogel "glue" [21]. Figure 4 depicts four different examples of bone graft substitutes.substitutes.

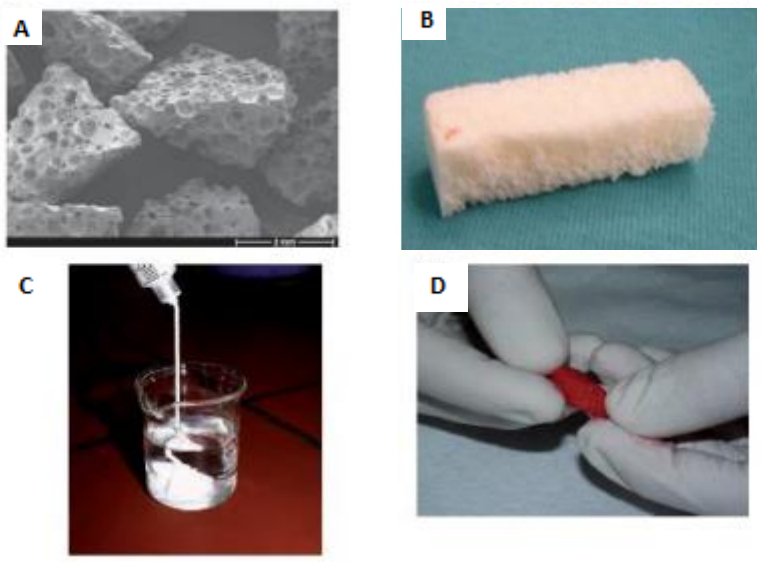

Figure 4- Four main types of bone graft substitutes: a) granule; b) block; c) cement; d) putty [18, 46].

2.6. Bone grafts and substitutes: Market analysis

The aging population is a key driver of growth in the bone grafts and substitutes market, as the prevalence of orthopedic and spinal disorders, such as osteoporosis' consequences, osteoarthritis, and spinal degeneration, increases with age. The growth of the market is driven by several factors such as the increasing incidence of musculoskeletal disorders, rising demand for minimally invasive procedures, technological advancements in the development of bone grafts and substitutes and increasing investments in research and development activities [34, 35].

According to a market research report by Grand View Research, the global bone grafts and substitutes market was valued at USD 3.06 billion in 2022 and is expected to

reach USD 4.94 billion by 2030, growing at a rate (CAGR) of 6.2% during the forecast period 2022-2030. The Centers for Disease Control and Prevention (CDC) report forecasts a significant increase in the global incidence rate of hip fractures, with an estimated 240% increase in women and 310% increase in men. Osteoporosis is also a concern, as it is estimated to impact approximately 200 million women across the globe. Additionally, the market for bone grafts and substitutes is expected to experience growth due to the growing demand for dental bone grafts in the coming years [36].

Geographically (figure 5), North America is the largest market for bone grafts and substitutes due to the presence of many key market players, increasing geriatric population, and a well-established healthcare infrastructure and global companies. However, the Asia-Pacific region is expected to witness the highest growth rate during the forecast period due to increasing investments in healthcare infrastructure, rising healthcare expenditure, and the increasing prevalence of orthopedic disorders [34, 35].

Figure 5- Growth rate by region- Bone graft and substitutes market [34].

In the United State of America, the spinal fusion segment dominated the market, accounting for over 60% of the revenue share, like its represented in the figure 6 below. The market is divided into various applications such as joint reconstruction, foot and ankle, spinal fusion, craniomaxillofacial, dental, and long bone. The growth of the spinal fusion segment is due to the increasing use of bone graft materials for spondylosyndesis and the rising incidence of orthopedic ailments among the elderly population [36].

The dental segment is expected to experience a significant boost in growth in the forecast period due to the increasing use of bone grafts for dental procedures such as bone regeneration and dental implant surgeries. The success rate of dental implant surgeries is increasing, which has resulted in a growing demand for bone grafts and substitutes. The joint reconstruction segment is also expected to witness steady growth in the future due to the rising number of knee and hip replacement surgeries. Furthermore, the long bone segment is predicted to have significant growth in the coming

years due to the increasing number of injuries and traumas to extremities caused by road accidents and sports injuries [36].

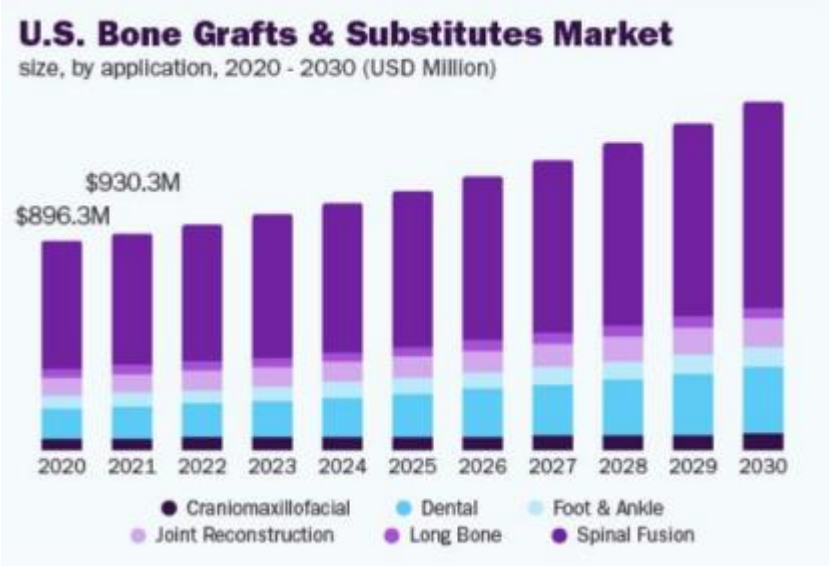

Figure 6- United States bone graft and substitutes market, growth rate by material type (2020-2030) [35].

The major players in the bone grafts and substitutes market include Zimmer Biomet Holdings, Inc., Medtronic plc, Stryker Corporation, Wright Medical Group N.V., NuVasive, Inc., Globus Medical, Inc., Johnson & Johnson (DePuy Synthes), Baxter International Inc., AlloSource, and Integra LifeSciences Corporation. These companies are focusing on product innovation, strategic partnerships, and mergers and acquisitions to expand their market share and strengthen their position in the market [36].

3. Methodology

3.1. Materials

The first goal of this work was to produce monophasic granules of HAp, with different sizes (nanoXIM•G1000 and nanoXIM•G2000) using the production process developed by FLUIDINOVA. Once the monophasic HAp granules were produced, their physicochemical and mechanical properties were analyzed. This included studying their composition, structure, surface properties, and mechanical strength. The objective was to gain a comprehensive understanding of the characteristics and behavior of these material. Building upon the monophasic HAp granules, the study aimed to produce biphasic granules consisting of both HAp and ß-TCP, where different proportions of these two phases can be explored to evaluate their impact on the properties of the granules. The physical, chemical, and mechanical properties of the biphasic granules were also analyzed, with the objective to assess how the addition of the ß-TCP phase influenced the overall properties of the granules, and whether they exhibited advantages in terms of their potential applications for bone regeneration.

The main specifications and properties of these granules are represented in table 1 and 2, respectively [37].

Table 1- Main specifications of FLUIDINOVA's HAp granules. Adapted from [37].

Product specifications	Product	Specifications
Size range	nanoXIM•G1000	0.5 -1.0 mm
	nanoXIM•G2000	1.0 – 2.0 mm

Table 2- Main properties of FLUIDINOVA's HAp granules. Adapted from [37].

General Properties	Product	
Physical appearance	nanoXIM•G1000	White spherical granules
	nanoXIM•G2000	White spherical granules

3.1.1. FLUIDINOVA's Hydroxyapatitite

The HAp ($Ca_{10}(PO_4)_6(OH)_2$) used to produce the granules was a powder consisting of micrometric aggregates of synthetic HAp nanoparticles, called nanoXIM•HAp202 from FLUIDINOVA S.A. This commercially available powder has a phase purity of 100%, a bulk density of 0.50 ± 0.10 g/cm^3, and a particle size (d50) of 5.0 ± 1.0 µm. The properties of this powder are listed in the table 3 below [38].

Table 3- Properties of FLUIDINOVA's nanoXIM•HAp202 HAp. Adapted from [38].

HAp nanoXIM•HAp202	
Purity (%)	100
Heavy metals (ppm)	≤ 20
Particle size d50 (µm)	5.0 ± 1.0
Bulk density (g/cm^3)	0.50 ± 0.10

3.1.2. FLUIDINOVA's ß-TCP

Table 4- Properties of FLUIDINOVA's nanoXIM•TCP600 B-TCP. Adapted from [39].

B-TCP nanoXIM•TCP600	
Purity (%)	≥ 95
Heavy metals (ppm)	≤ 30
Particle size d50 (µm)	≤ 15
Bulk density (g/cm^3)	≥0.4

The ß-Tricalcium phosphate (ß-TCP) used for this research was a pre-calcined ß-Tricalcium phosphate (nanoXIM•TCP600), $Ca_3(PO_4)_2$, provided by FLUIDINOVA S.A. It exhibits a minimum phase purity of 95%, a maximum particle size (d50) of 15 µm, that is half of the granules have diameters less than or equal to 15 µm. The properties of this powder are listed in the table 4 below [39].

3.1.3. Sample's Preparation

Firstly, before the production of biphasic granules, the focus was on producing monophasic granules of HAp. The objective was to gain a better understanding of the production techniques, examine their morphology, and study and determine the physicochemical and mechanical properties of this bioceramic with different sintering temperatures. Table 5 shows the produced batches.

Table 5- Designation of each batch of HAp granules produced and the sintering temperatures used.

Batch	HAp1000	HAp1100	HAp1200	HAp1300
Sintering Temperature (°C)	1000	1100	1200	1300

To produce the biphasic granules, it was considered a previous work performed at FLUIDINOVA [40]. Therefore, the samples containing a ratio of 75% HAp and 25% β-TCP were selected for further investigation due to their insufficient mechanical resistance at 1000 °C. In general, in this previous work, all the formulations used obtained adequate mechanical strengths, except this one. Consequently, this specific formulation required improvement, so various sintering temperatures were tested, to analyze and study their physicochemical and mechanical properties, as illustrated in the table 6 provided below.

Table 6- Designation of each batch of biphasic granules produced and its composition.

Batch	Bp1000	Bp1100	Bp1200	Bp1300
HAp/β-TCP Ratio (%)	75/25	75/25	75/25	75/25
Sintering T (°C)	1000	1100	1200	1300

3.2. Experimental Procedure

The provided flow chart illustrates the production process for nanoXIM granules, accompanied by an explanation for each individual stage.

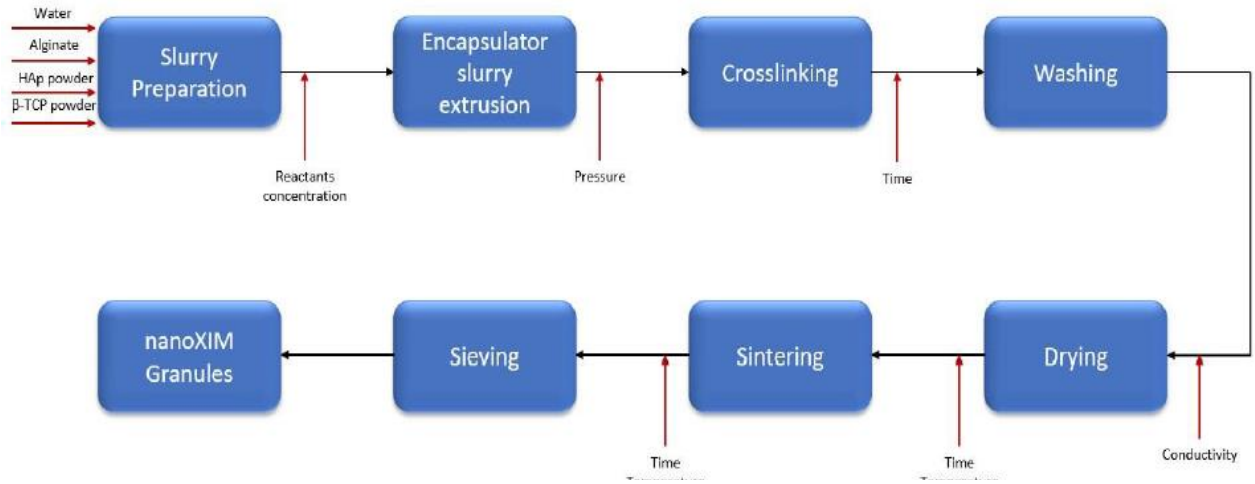

Figure 7- Flow chart of the production process for nanoXIM granules [40].

3.2.1. Slurry Preparation

To produce the spherical granules, first it was prepared a slurry consisting of alginate that was dissolved into pure water, under agitation with a mechanical stirrer (figure 8). After complete dissolution of alginate, when the slurry acquires a slightly viscous consistency and yellowish color, it was possible to add the HAp and ß-TCP powders into it. For the monophasic granules, only the nanoXIM•HAp202 product was gradually added to the solution until a completely homogeneous slurry was obtained. For the biphasic granules, in a previous work performed at FLUIDINOVA, a calibration line was elaborated to know which amount of each bioceramic powder must be added to achieve a desired final ratio of HAp and ß-TCP, in this case a ratio of 75/25. The amount of reagents and the calibration line is FLUIDINOVA's intellectual property and therefore cannot be presented in this work.

Figure 8- Slurry preparation using a mechanical stirrer.

3.2.2. Slurry extrusion

The lab-scale encapsulator system, shown in figure 9, oversees producing spheroidal droplets by extruding the slurry. This shape is achieved by pushing it through a needle located at the end of the encapsulator. Firstly, the assembled system was fully washed with water. The slurry was then transferred to a Schott flask, ensuring that the tubes were properly connected to the encapsulator. To start the process, the flask was subject to a normalized pressure of 0.1 bar, applied at the encapsulator tip, close to the needle, to regulate the diameter of the spheres. Without this pressure, the droplet size is only affected by the diameter of the needle and gravity force. By employing this method, it becomes feasible to create droplets with a wider range of diameters. Consequently, increasing the pressure results in the production of droplets with smaller diameters. For both granules (nanoXIM•G1000 and nanoXIM•G2000), the procedure was the same, however the encapsulator is different, as it can be observed in figure 9.

Figure 9- Spheres' production method. A) nanoXIM•G1000 granules' encapsulator; B) nanoXIM•G2000 granules' encapsulator.

3.2.3. Crosslinking

After the slurry reaches the encapsulator, it was extruded into multiple droplets, which fall into the calcium chloride solution ([CaCl2] = 0.1 M), instantly forming the spheres. This phenomenon occurs due to the quick formation of calcium-based connections between poly-guluronic acid sequences along the polymer chain, which results in spherical particles that comprise an alginate hydrogel structure with embedded ceramic particles. Verifying the extent of crosslinking was crucial, so the spheres were allowed to settle for 30 minutes (figure 10), ensuring their stability during subsequent stages of production.

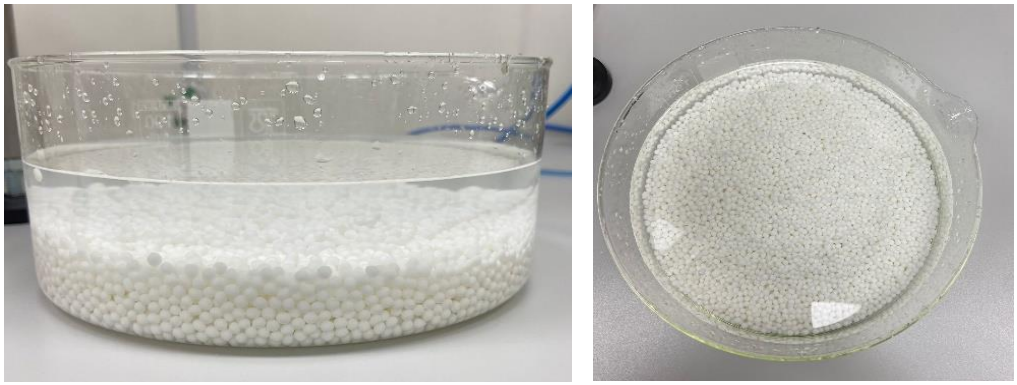

Figure 10- Spheres' formation into the calcium chloride solution.

3.2.4. Washing

After the crosslinking process, the calcium chloride solution was discarded, carefully decanted or using a sieve, and the spheres are washed multiple times with deionized water. This process is important due to the higher concentration of salts in this solution, which may be dangerous for the patient upon clinical application. The spheres were considered washed when the conductivity is below a normalized value, 700 µS/cm, measured by an electrical conductivity meter (EC meter), to ensure that the remaining salts in the solution do not cause any disruption during the production of the spheres or affect their final properties.

3.2.5. Drying

Then the last wash water was poured, the spheres were immersed in an ethyl alcohol layer to prevent them from agglomerating during the drying step. Afterward, the spheres were placed into an oven to eliminate the water before the subsequent sintering stage. For this, the spheres were subjected to a drying process at 105ºC overnight.

3.2.6. Sintering

After drying, the spheres were removed from the drying oven and placed into a sintering oven, in alumina crucibles, to be submitted to a sintering process. This process was split into three phases. In the first phase, the spheres were heated gradually at a rate

of 5 °C per minute until the temperature at which the sintering will be performed is reached, to prevent thermal shock and disintegration of the spheres, ensuring complete removal of residual humidity left from the drying process and also the beginning of alginate degradation. The second stage involved sintering the spheres for 2 hours at a temperature of 1000 °C, 1100 °C, 1200 °C and 1300 °C, where the alginate that makes up the spheres is entirely eliminated, resulting in fully bioceramic spheres. In the final stage, the granules were slowly cooled inside the furnace.

3.2.7. Sieving

The spheres were taken out of the furnace, completely cooled down and transferred to a sieving column. This column separates the spheres based on size: the nanoXIM•G1000 spheres must stay between the 0.5 mm and 1 mm sieve size, and between 1.0 and 2.0 mm for the nanoXIM•G2000, that are collected in containers for further analysis. Any spheres that fall outside of these size ranges were also collected and kept separately for X-ray diffraction (XRD) analysis since this type of analysis is not dependent on the particle size.

3.3. Granules Characterization

3.3.1. Scanning Electronic Microscopy

The monophasic granules produced in this work underwent analysis using scanning electron microscopy (SEM). This test was done to analyze not only the shape, geometry and size of the granules, but also the size of the existing pores. The analysis was performed at the *Centro de Materiais da Universidade do Porto* (CEMUP) using a high-resolution Scanning Electron Microscope called Quanta 400FEG ESEM/EDAX Genesis X4M. In order to prepare the samples for the analysis, they were placed on an aluminum support and secured with carbon tape and pre-assembled on araldite. Subsequently, a thin gold/palladium film was applied to the samples using cathodic pulverization to provide conductivity.

3.3.2. X-Ray Diffraction

The purpose of the X-Ray diffraction analysis was to determine the crystalline phases present on the granules and their crystallinity and the XRD patterns were refined using the Rietveld method. This analysis was carried out at FLUIDINOVA, S.A., where all samples, both monophasic and biphasic, underwent the analysis with the same conditions. A Rigaku Miniflex 450 was used with a D/teX Ultra2 detector, Cu-Kα radiation (λ = 1.54059 Å) and an energy of 30 kV and 15 mA. The acquisition was performed between 8° < 2θ < 80°, with a step size of 0.01° and a speed of 1°/min. The *SmartLab Studio II* software was used for phase identification and quantification.

3.3.3. Linear and Volume Shrinkage

During sintering the granules densify, which leads to a decrease in their levels of porosity, macroporosity and microporosity, along with linear and volumetric contraction. Additionally, the heat treatment used, promotes the completely burn of the alginate presents in the granules.

By using Equations 1 and 2, it was possible to calculate the extent of linear and volume shrinkage after sintering, respectively. For this, the diameter of 40 granules was measured with the aid of the magnifying glass and *ImageJ* software. The volume was then calculated ($V = 4/3\ \pi\ r^3$) with these values, where it was assumed that the granules were perfect spheres.

$$\%\ Linear\ Shrinkage = \frac{d_{initial} - d_{final}}{d_{initial}} \times 100 \qquad \text{Eq.1}$$

$$\%\ Volume\ Shrinkage = \frac{V_{initial} - V_{final}}{V_{initial}} \times 100 \qquad \text{Eq.2}$$

3.3.4. Bulk density

The bulk density method was the process chosen to calculate the density of the granules, obtained by the ratio of the mass of a certain quantity of granules to its volume. For this, it was used a graduated cylinder, which was filled with granules, without compacting, to a volume of 15 mL and the mass was measured. After that, the tapped density technique was employed, which involves mechanically tapping a graduated powder sample to achieve an increased bulk density. Once the initial mass of the granules was observed, the measuring cylinder underwent mechanical tapping, with the equipment at figure 11, and volume readings were taken until significant volume change was observed. It was carried out 500, 1250 and 2500 taps on the same sample and the corresponding volumes V_{500}, V_{1250} and V_{2500} were recorded to the nearest graduated unit. If the difference between V_{500} and V_{1250} is 2 mL or less, then V_{1250} was considered the tapped volume. However, even if after 1250 taps no volume change occurs, it was necessary to perform 2500 taps, and V_{2500} was considered the tapped volume. The process was repeated to make three tests for each sintering temperature used [41].

Finally, the specific weight was calculated in grams per milliliter using the formula $\boldsymbol{m/V_f}$, where V_f is the final tapped volume. Then the relative density was calculated, (measure of the density of a substance in comparison to the density of water.). In addition, the apparent densification and the overall porosity were calculated from the

equations 3 and 4, respectively.

$$Apparent\ densification\ (\%) = \frac{calculate\ density}{theorical\ density} \times 100 \qquad \textbf{Eq.3}$$

$$Global\ porosity\ (\%) = \frac{theorical\ density - calculate\ density}{theorical\ density} \times 100 \qquad \textbf{Eq.4}$$

Figure 11- Equipment used for the mechanical tapping to calculate the bulk density.

3.3.5. Inductively Coupled Plasma – Atomic Emission Spectrometry (ICP- AES)

During the performed work, a change in the color of the granules with sintering temperature was seen, which will be explained in more detail further in this document. However, to analyze this change, an analytical technique called Inductively Coupled Plasma – Atomic Emission Spectrometry (ICP- AES) was employed in 9 different samples in the form of powder: one of each raw material (calcium, phosphorus and potassium sources), another of the HAp powder used, and 5 samples of granules produced at different sintering temperatures. This method enables the simultaneous quantitative and qualitative analysis of multiple elements in the batches. The underlying principle involves using plasma, created by strongly ionized and electrically neutral argon gas, as the atomization source. To conduct the analysis, a Horiba Jobin-Yvon Ultima radial observation instrument was utilized. This instrument was equipped with a 40.68 MHz RF generator and a 1.00 mm Czemy-Turener monochromator. The data acquisition and equipment control were facilitated by *JY v5.4* software.

3.3.6. X-Ray Photoelectron Spectroscopy (XPS)

The change in color observed in the samples with increasing sintering temperature raised various concerns, one of which being the influence of the furnace

atmosphere. As a result, XPS analysis was required to determine the oxidation state of the elements contained in the samples and their potential impact on the generation of pinkish color. The XPS method enables elemental chemical analysis from the top layer of a sample's surface, which has a thickness of less than 10 nanometers. To ensure accurate results, the surface must be completely clean and free from any contaminants. To conduct this analysis, the samples need to be compatible with an ultra-high vacuum environment ($<10^{-6}$ Pa).

In this case, four thin pellets were carefully prepared by compressing different powders: one from the HAp1000 sample, another from HAp1200, and two from HAp1300. For this, the equipment used was Kratos Axis Ultra HAS equipped with a monochromatized aluminium X-ray source running at 15 kV. The analyses were conducted using the hybrid lens mode with the slot aperture, with the analyzed area measuring about 300 µm x 700 µm. The pass energy was configured to 160 eV for the survey spectrum and 40 eV for more detailed scans. The Vision software was employed for data acquisition and equipment control, while CasaXPS software was utilized to simplify data analysis.

3.4. Mechanical Characterization

3.4.1. Compression Tests

The compression tests were carried out with the aid of the equipment Compact Tabel-Top Universal / Tensile Tester from Shimadzu (figure 12). It used a 500 N load cell and a speed of 2 min/mm. For this, 10 individual granules (nanoXIM•G2000) for each batch (HAp1000, HAp1100, HAp1200, HAp1300) were subjected to testing, and their diameter was measured using a caliper.

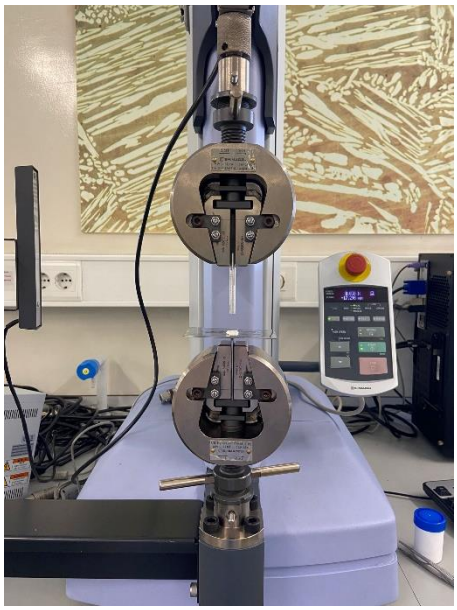

Figure 12- Equipment, Compact Tabel-Top Universal / Tensile Tester from Shimadzu, used in this work.

The tensile strength, σ (MPa) was calculated by using equation 5, mentioned above, where *F* represents the failure load (N) and *R* (mm) the granule's radius [42].

$$\sigma = \frac{F}{2 \times \pi \times R^2} \qquad \textbf{Eq.5}$$

3.4.2. Vickers Hardness Tests

These tests can be used to evaluate the mechanical properties of the materials, such as their resistance to deformation and fracture. For these, the equipment required was FALCON 400 micro/macro-Vickers hardness tester (INNOVATEST), where a load of 1 kgf was applied to the surface of the HAp samples (HAp1000, HAp1100, HAp1200, HAp1300) by a diamond indenter for 15 seconds. To perform the tests properly, since it would be difficult to do it on a single granule, the sintered samples were embedded into epoxy molds and polished, until the resin is completely removed from the surface, and the granules are visible. Then, it was made 10 indentations for each sample, and they were analyzed to determine their hardness. It was determined by measuring the length of the diagonal ident shape, formed after the indentation on the surface of the sample, which was given by the test software.

Despite that, to validate the results obtained from the software, the samples were subjected to SEM analysis, allowing for visual identification of the indentations.

3.5. Statistical analysis

To assess whether there were any significant statistical differences among the obtained results, a thorough statistical analysis was conducted using Student's t-test. The results were considered statistically different when the p-value was less than 0.05. The presentation format for all the results includes the mean value accompanied by its corresponding standard deviation.

4. Results and Discussion

4.1. Granules Characterization

4.1.1. Monophasic Granules

4.1.1.1. Granules color

During the production of the HAp granules, a difference in color was evident with the different sintering temperature used. As can be seen in the image below (figure 13), with an increase in temperature, the granules change from white color to a pinker shade. Several treatment conditions were tested, namely the number of granules in the crucible and the use or not of a lid on it, since it was possible to observe that the furnace atmosphere would also be an important parameter to control, as there was a belief that the color might be attributed to the oxidation of certain elements during the sintering process. Given the ultimate purpose of their application, it is crucial to determine the cause of this color alteration to prevent possible negative consequences for commercialization. Therefore, considering all these adjustments, it proved to be a difficult task to ascertain the origin of the problem. As a result, further tests and analyses were carried out to find the underlying cause.

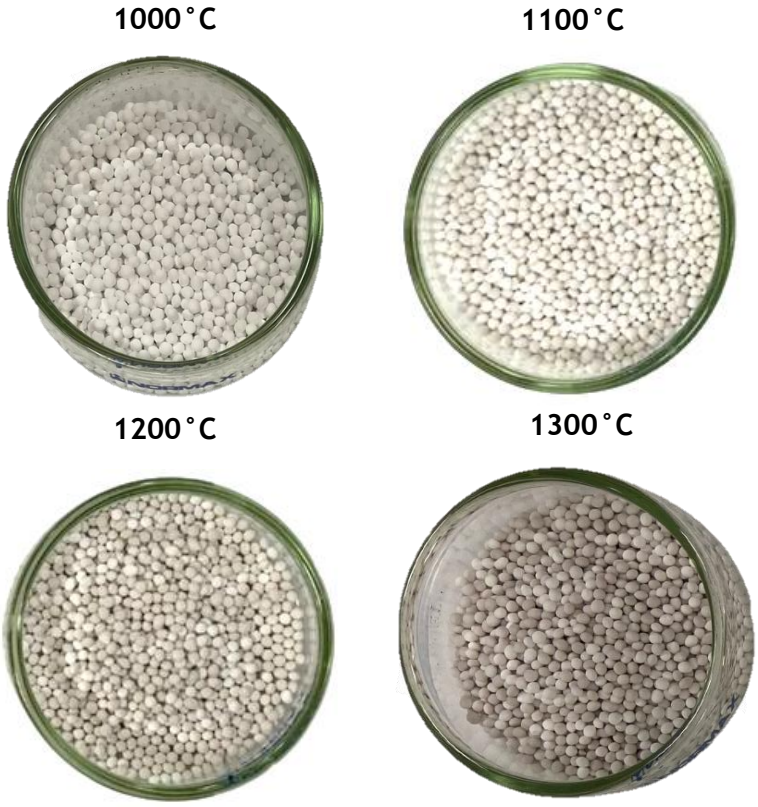

Figure 13- Color change of HAp granules from white to pink color when increasing the sintering temperature.

4.1.1.2. Scanning Electronic Microscopy

HAp possesses an exceptional appeal due to its outstanding biocompatibility and bioactivity, making it a vital constituent for biomedical applications. The optimization and utilization of these properties are greatly dependent on critical material characteristics such as particle size, dimensional anisotropy, morphology, real microstructure, and others [43]. The constraint of bone graft replacements with specified shapes is overcome by using granular bone substitutes, which can be applied in bone defects of diverse sizes and shapes.

A spherical morphology makes surgical implantation simpler and enables the adoption of less intrusive methods with more controlled flowability. Additionally, spherical enhances packing into the defect and produces a consistent intergranular macroporosity that encourages effective osteoconduction. On the other hand, irregular particles produce a more heterogenous packing inside the defect, which may hinder vascularization and the development of new bone while also triggering an inflammatory response [44].

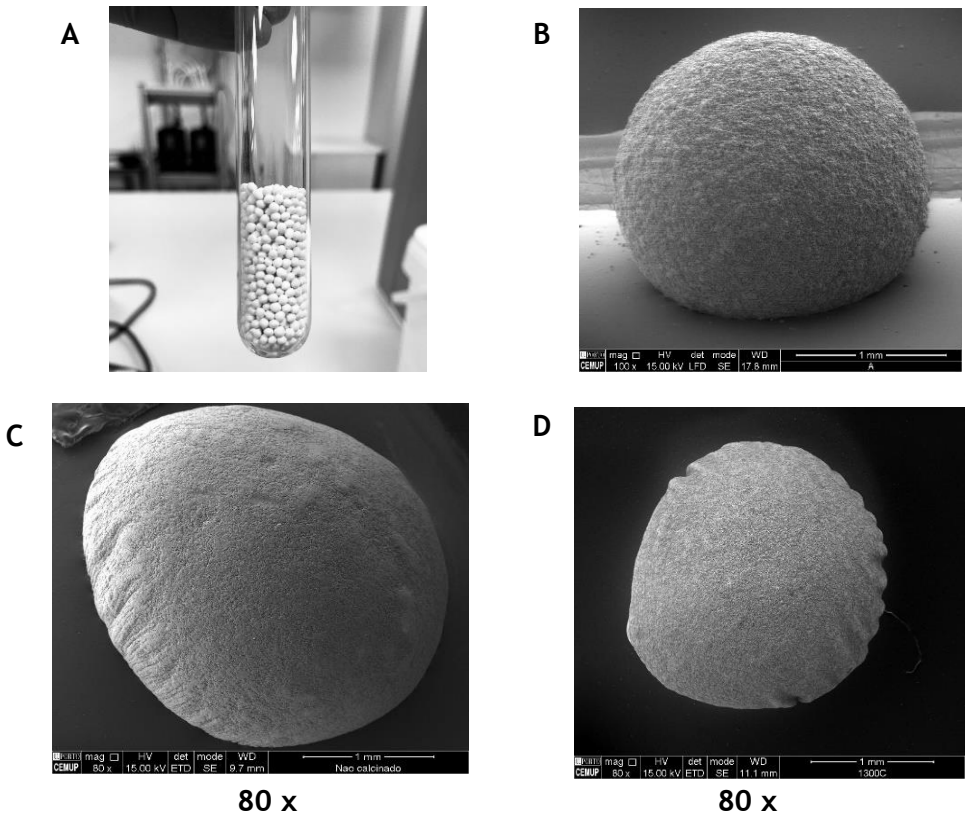

Figure 14-A) Macroscopic view of the HAp granules; B) Spherical shape of the granules; Images obtained through SEM relative to C) Before sintering and D) HAp1300 (after sintering), that provide a perspective of the granules, clearly displaying their spherical shape and size.

So, before analyzing the biphasic properties, it is essential to comprehend the influence of different processing conditions on the particle size and morphology of the granules. The effects of different heat treatments on the morphology of spherical granules were observed using SEM, as depicted in figure 14. Figure 14A provide a macroscopic view of the granules, figure 14B their spherical shape, and figure 14C and 14D highlighting their size. Surface details of HAp spherical granules are illustrated in figure 15.

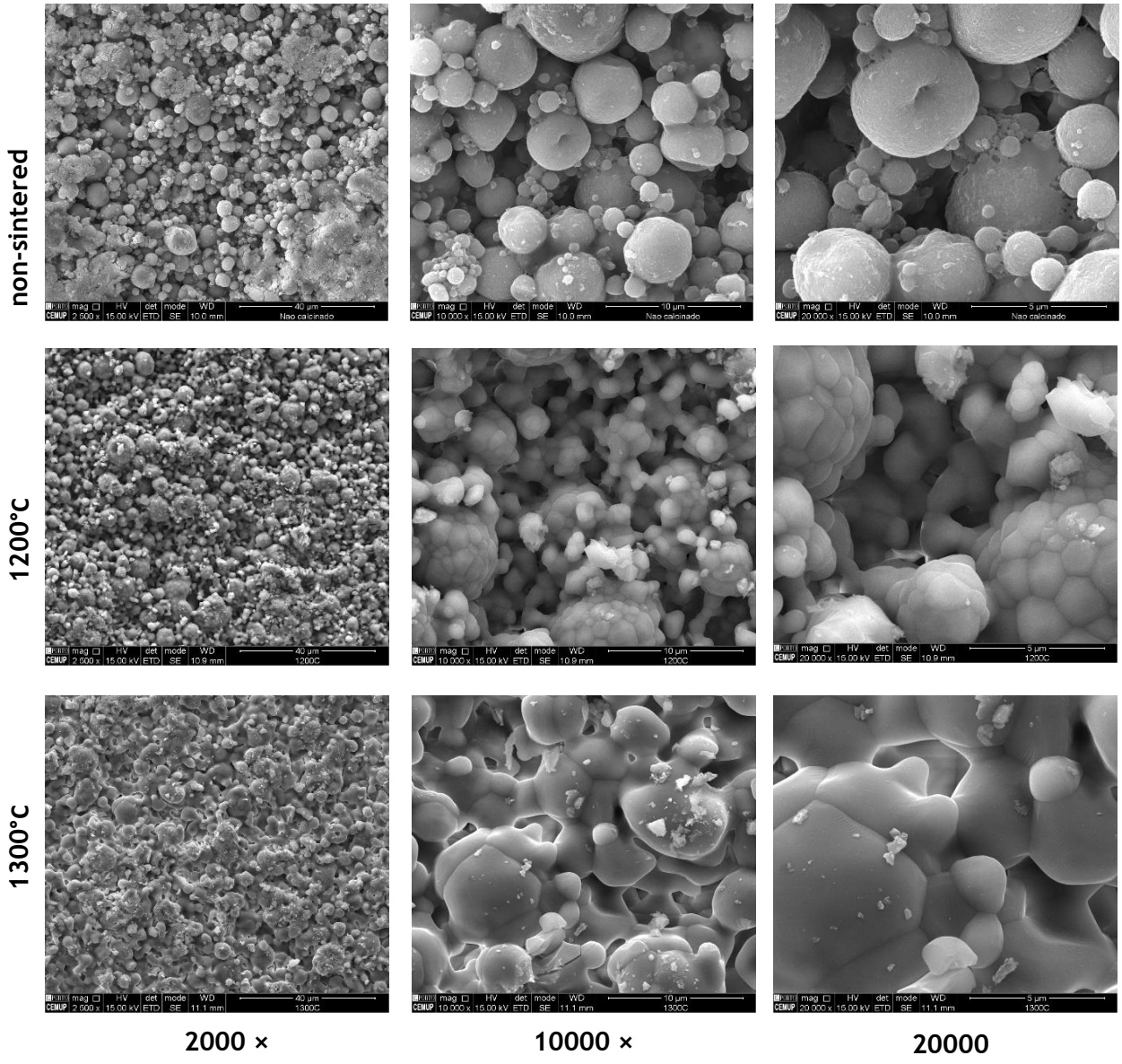

Figure 15- SEM images reveal the surface characteristics of non-sintered HAp spherical granules and sintered at temperatures of 1200 and 1300 °C.

Firstly, upon examining figure 14C and 14D, it is evident that the sintering temperature may lead to a reduction in granule size. To substantiate this observation, measurements of their diameters were conducted using the image analysis software, *Image J*. The obtained values confirmed this hypothesis, where 2.60 mm represented the non-sintered HAp granule diameter (figure 14C) and 2.06 mm (figure 14D) represented the HAp1300 measured value, which means that has a reduction on the diameter of 20.77%.

As expected, the elevated temperature causes the particles within the granules to bond, leading to a reduction in the number of pores.

As can be seen in figure 15, it became evident that increasing the sintering temperature led to the coalescence of HAp crystals, like it was mentioned before. Consequently, the contact between crystal aggregates was significantly improved due to increased atomic diffusion, which promotes their bonding and the increased of compressive strength. It is also possible to observe the zones where the particles meet each other, and from where their nuclei start to come closer together.

Using SEM, four measurements of pores were performed on the samples without any heat treatment and HAp1300 (figure 16), obtaining an average of pore size equal to 2.54 µm and 2.27 µm, respectively. This indicates the reduction in microporosity with the increase in sintering temperature, due to particles coalescence. However, spherical granules sintered at lower temperatures display nanoporosity on their surface, that arises from the raw materials powders.

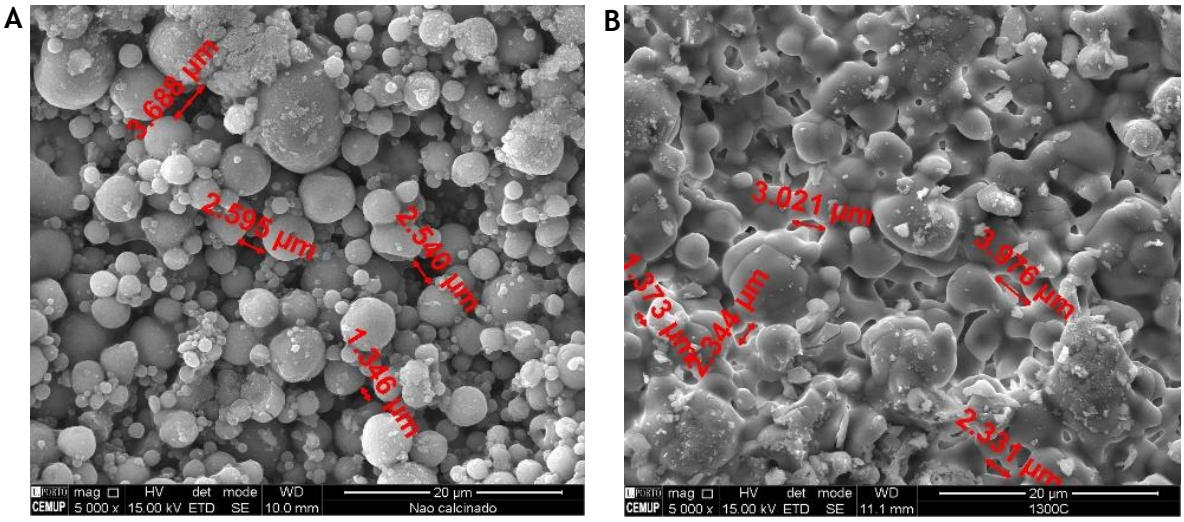

Figure 16- SEM images with the measurements of pores sizes on the samples A) non sintered and B) HAp1300.

In figure 17, it is possible to observe representative SEM images that were obtained for the batches HAp1000 and HAp1300. In general, a significant disparity in particle size within the granules can be observed in both samples. In figure 17A, a larger number of particles with different sizes can be seen, giving the appearance of a looser arrangement. However, as the temperature increases, these particles gradually start to bond, or coalesce (figure 17B), which proves the increase of the particle size, and their densification.

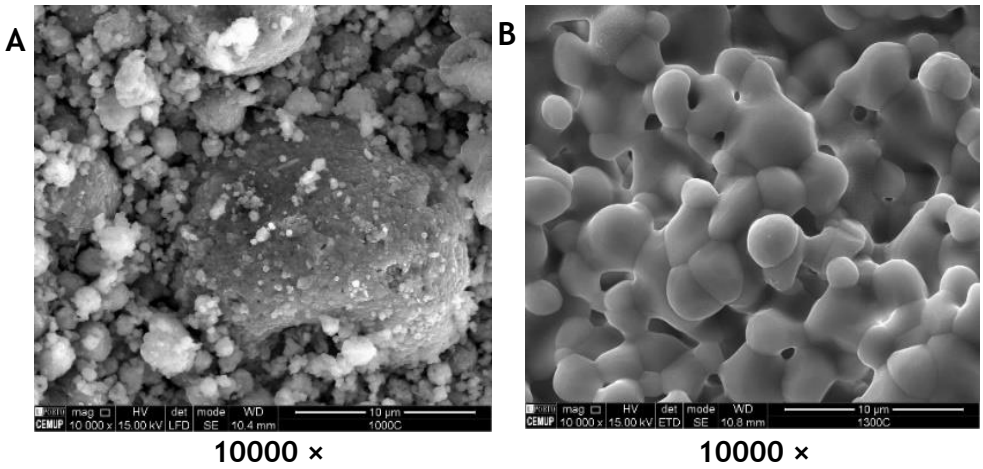

Figure 17- SEM images of A) HAp1000 and B) HAp1300.

4.1.1.3.X-Ray Diffraction

To determine the crystallographic phases and assess the level of crystallinity in the produced granules, an X-ray diffraction analysis was conducted on the monophasic batches. In figure 18, XRD spectra for HAp spherical granules sintered at 1000 °C (batch HAp1000) may be observed. The diffractogram in the figure above is also representative of HAp1100 and HAp1200 batches.

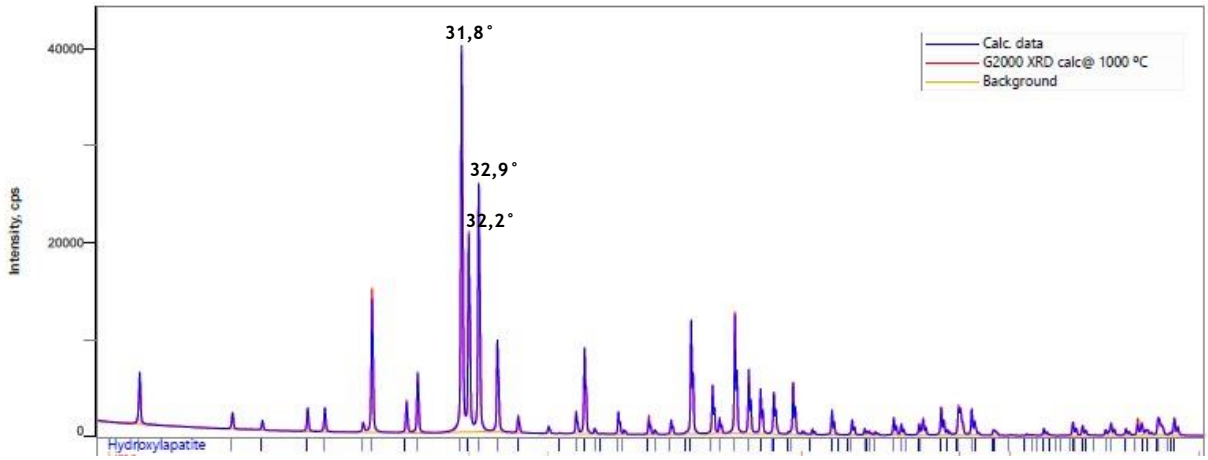

Figure 18- Diffractogram obtained through X-Ray diffraction analysis of HAp1000.

According to literature, there are three main identification peaks at 2θ = 31.8° (211); 32.2° (112); and 32.9° (300) used for pure HAp identification, the first being the one with the highest intensity [45]. By analyzing the diffractograms exhibited in Figure 18, it was possible to conclude that HAp1000, HAp1100 and HAp1200 have high crystallinity since their characteristic peaks are very narrow, with an average phase purity of 98.99%. However, XRD also detected the presence of calcium oxide (CaO) in very small percentages (1% approximately), which is expected given that this phase is likely to be

present in the granules' composition due to the powder production process.

In another hand, figure 19 represents the HAp1300 diffractogram. After its analysis, it is possible to conclude that HAp1300 has a high level of crystallinity because of the notable narrow distinctive peaks. However, there is an appearance of a previously undetected phase, tetracalcium phosphate, $Ca_4O_9P_2$ (TTCP). This was expected since HAp (not pure phase) undergoes a phase transformation at typical sintering temperatures above 1100 °C. In general, HAp goes through phase instability at high sintering temperatures, where HAp can lead to its partial thermal decomposition into $Ca_4O_9P_2$, TCP and/or TTCP [42, 43]. In the graph in figure 20, it is possible to observe the amount of each phase existing in HAp1300: 92.15% of HAp and 7.85% of TTCP.

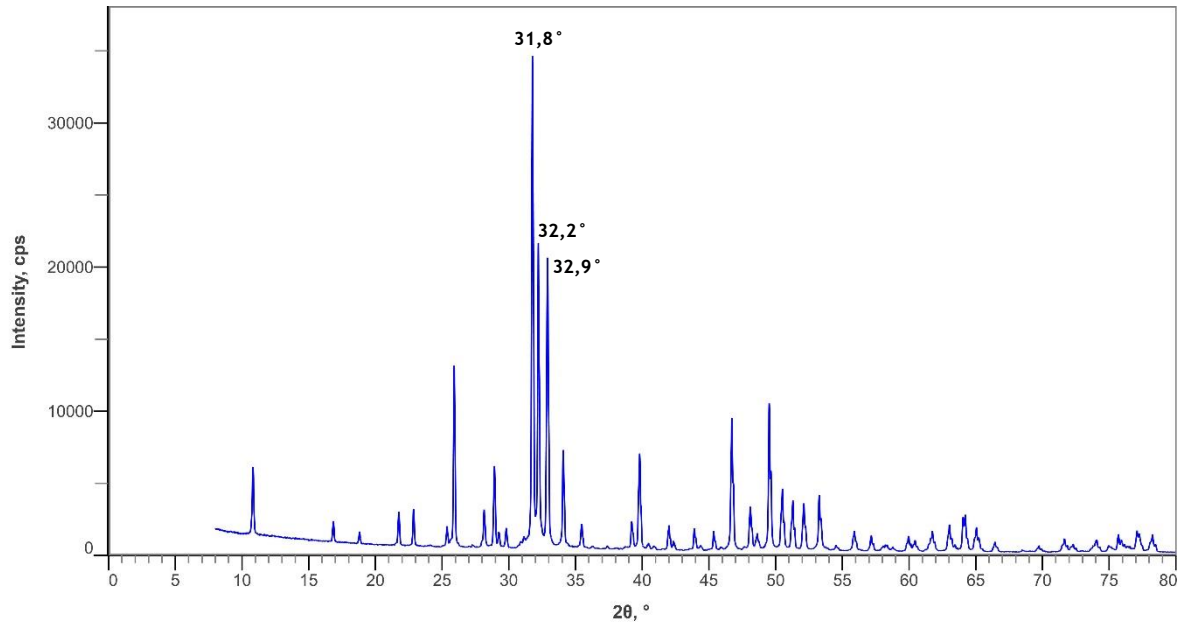

Figure 19- Diffractogram obtained through X-Ray diffraction analysis of HAp1300.

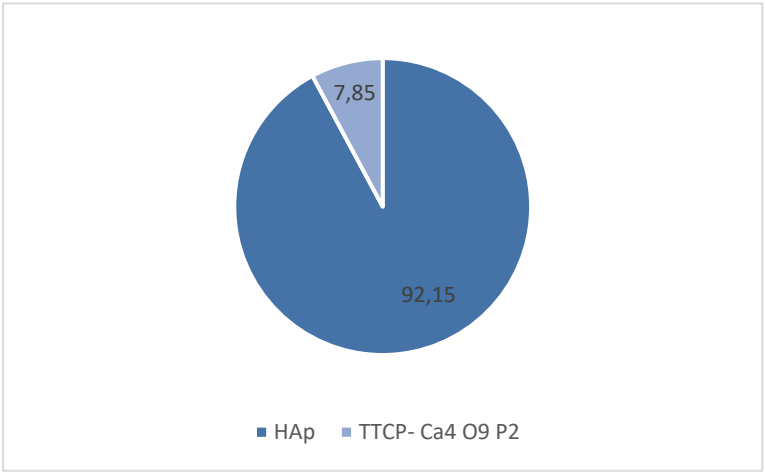

Figure 20- Weight fraction of existing phases in HAp1300.

This calcium orthophosphate (TTCP) is the most basic one, however its solubility in water is higher than that of HAp. It cannot be formed by precipitation from aqueous

solutions but requires a solid-state reaction at temperatures above 1300 ºC for synthesis. TTCP exhibits limited stability in aqueous environments, as it undergoes gradual hydrolysis to form HAp and calcium hydroxide. Due to this hydrolysis process, TTCP is not typically present in biological calcifications [47]. For these reasons, sintering should not be carried out at such high temperatures, so that the HAp does not decompose. The production of biphasic granules composed of HAp and ß-TCP are a better alternative to avoid the formation of this phase and are studied later in this work.

4.1.1.4. Linear and Volume Shrinkage

It is important to understand the method of production, and how its different stages and parameters influence the granules' particle size and morphology. For this, and to prove the densification of the granules and in turn the decrease in their porosity level with increasing sintering temperature, the volume of the HAp samples was calculating by measuring their diameter. Then their linear and volume shrinkage after sintering were calculated.

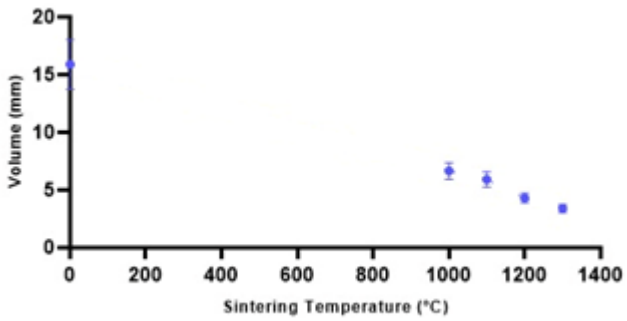

Figure 21- Granules' volume evolution with sintering temperature of each batch.

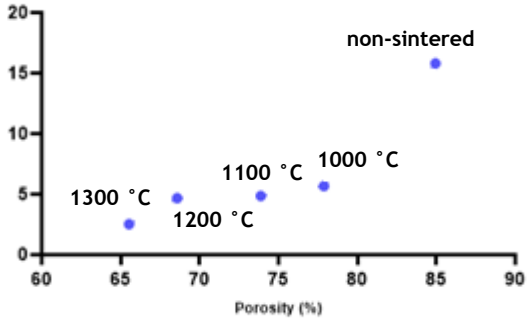

Figure 22-Granules' average volume evolution with average porosity of each batch.

Figure 21 represents the behavior of the mean value of the calculated granules' volumes as a function of sintering temperature. As expected, with increasing temperature there is a significant decrease in the size of the granule. This is justified due to the presence of alginate in their structure, since the granules were subjected to a high enough temperature that promotes the burning of the alginate, which results in a decrease of their size. Furthermore, as could be seen in the SEM images, the particles tend to coalesce with increasing temperature and consequently decrease the number of existing pores, which will decrease the granule size.

Furthermore, in figure 22, a graph illustrates the relationship between the average of percentage of the existing pores on each sample, with their corresponding sintering temperature, and the average volume evolution of them. As anticipated, with lower sintering temperature, the global porosity increases and consequently, the volume of the granules increases too. This outcome can be attributed to the bonding of particles within the granules caused by the sintering temperature, resulting in a reduction in the

number of pores and consequent decrease in volume.

As it was mentioned before, the linear and volume shrinkage was calculated by using Equation 1 and 2, from 3.3.3. By calculating the average of the values for each batch, the linear shrinkage obtained was approximately 40,12±0,01 % and the volume shrinkage obtained was 78,51±0,01 %.

4.1.1.5. Bulk Density

As previously discussed, the density of bioceramics is influenced by the sintering process. By adjusting parameters during sintering, it is possible to achieve bioceramics with varying levels of density, including the physical features of both pores and grains (such as their shape, size, and distribution), the energy and movement of grain boundaries and pores on the interface and surface, and the primary mechanisms involved in sintering. Therefore, utilizing smaller powder particles to produce the green body results in higher bioceramic density [48].

Table 7 presents the relative density values obtained for each batch, along with their corresponding densification and global porosity, calculated by equations 3 and 4 from 3.3.4.

Table 7- Relative density values obtained for each batch, along with their corresponding global porosity.

Batch	HAp1000	HAp1100	HAp1200	HAp1300
Relative density	0.92 ± 0.005	1.03 ± 0.008	1.14 ± 0.014	1.31 ± 0.008
Apparent densification (%)	16.58 ± 0.16	20.67 ± 0.18	24.78 ± 0.37	30.99 ± 0.30
Global porosity (%)	70.79 ± 0.12	67.25 ± 0.21	63.48 ± 0.35	58.89 ± 0.20

Overall, and consistent to what was showed in the SEM images, the bulk density of the HAp samples tends to increase as the sintering temperature rises, leading to their densification when compared to the non-calcined samples. On the other hand, if the samples become denser, it is expected that the percentage of pores in the samples will decrease, as observed in the values presented. However, a larger number of tests would be necessary to obtain a larger sample size and thus draw statistically significant conclusions.

According to the literature, HAp presents a theoretical density value of 3.16

[49]. Nevertheless, the measured density of all the batches was approximately one-third of the anticipated values for complete densification, as indicated in Table 6. Therefore, it can be inferred that the sintering method employed for these granules did not achieve complete densification, resulting in the formation of structures with pores. This can be attributed to the release of alginate from the material's structure, which led to pore formation and also to the random packing of the powder particles within the granule. However, having a bioceramic with pores in a size range can be advantageous in terms of bone regeneration, since they facilitate quick bone growth into the material.

4.1.1.6. Inductively Coupled Plasma – Atomic Emission Spectrometry (ICP- AES)

The elementary composition of the samples was investigated with ICP-AES, and it was possible to analyze 33 different elements (appendix I). In order to compare the results obtained, FLUIDINOVA, S.A shared an analysis certificate of the raw materials used to produce the HAp powder. However, when the comparison was made, it was possible to conclude that some of the elements present in the ICP analysis were not analyzed by the raw materials manufacturers and therefore were not present in the certificate of analysis.

Table 8- Elements concentration (ppm) after ICP analysis**.**

	Elements concentration (ppm)			
Elements	**HAp1100**	**HAp1200**	**HAp1250**	**HAp1300**
B	27.00	26.00	27.00	29.00
Fe	6.24	6.79	7.56	6.43
Mg	12.70	12.80	12.50	13.80
Na	212.00	140.00	135.00	189.00
Si	42.30	41.90	42.00	45.30
Sr	58.00	59.00	59.00	61.00

In addition, it is known that the method used for the technical analysis is not ICP, so it is possible that the detection limit of elements is different. Thus, elements that are present in the raw materials as impurities or contaminants at very low concentrations may not be detected by the method used in the datasheet, as they are at concentrations below the datasheet detection limit. On the other hand, the data sheet may focus mainly on the main components or those considered most relevant for the specific use of the raw materials and not mention impurities in very low concentrations.

Moreover, traces of boron, barium, copper, iron, manganese, sodium, silicon and strontium were detected (table 8). Some of these elements were identified, but it was concluded that the color alteration could not be linked to their presence. This included copper (Cu), which was found in minimal amounts and therefore excluded as a potential cause. Barium (Ba), on the other hand, was present in significant concentrations but aligned with the information provided in the data sheets, thus ruling it out as a possible factor. Among the remaining elements, iron (Fe) and boron (B) were present in higher concentrations than expected. Further investigation revealed that these elements, when subjected to high temperatures, can form compounds that exhibit a slightly pinkish color, matching the observed color change. Therefore, it was necessary to perform further type of analysis to understand the influence of these elements on the color - the XPS analysis.

4.1.1.7.X-Ray Photoelectron Spectroscopy (XPS)

As previously mentioned, the alteration in color of the samples due to sintering temperature could potentially be attributed to the atmosphere within the furnace. So, to analyze the granules' elemental composition and their oxidation states, XPS analysis was performed. Through ICP analysis, it was possible to detect the presence of elements such as Boron (B) and Iron (Fe), which were in higher concentrations than expected, being these elements the focus of this analysis.

First, a general spectrum was acquired, from which the principal elements were identified (figure 23). By observing it, in addition to the expected elements, the presence of B or Fe was not detected as indicated by the peaks. Furthermore, it can be observed that the peak displaying the highest intensity corresponds to oxygen (O 1s), implying that this element is present in the largest quantity within our samples. This can be attributed to the oxygen-rich environment during the sample preparation and analysis. Despite the absence of Fe detection in the overall spectrum, considering the premise that this element was the primary cause of the samples' color change, the analysis time was extended to attain more detailed information. Subsequently, iron was successfully detected, albeit in minor quantities.

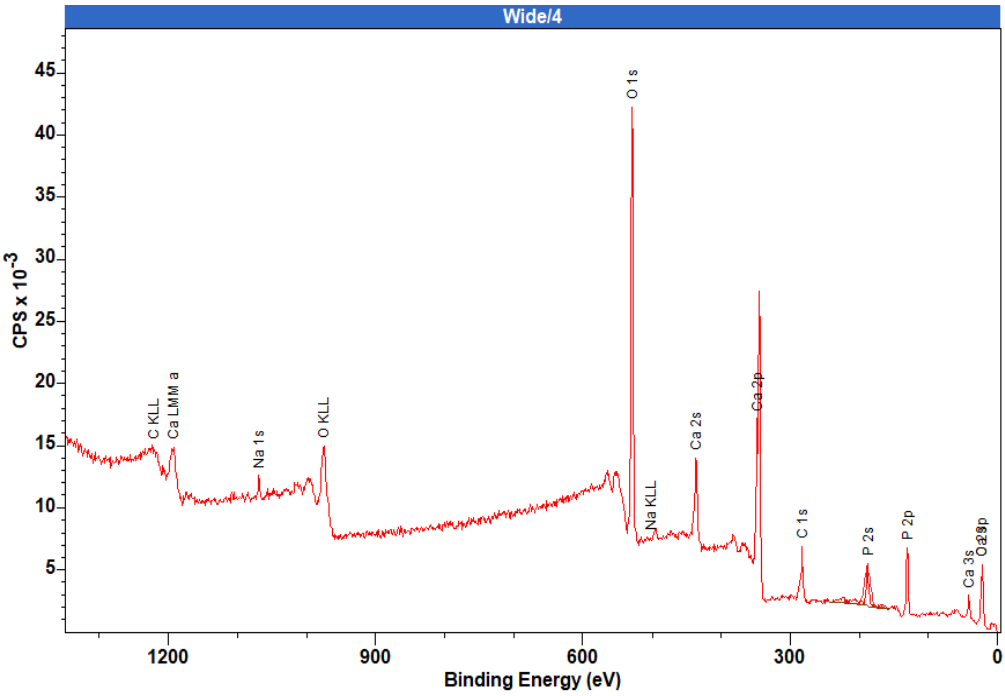

Figure 23- XPS global spectrum of HAp1200, being representative of all samples.

According to the literature, iron can exist in a variety of oxidation states (from +2 to +6), although the most common types found in nature are ferrous or ferric iron, Fe (II) or Fe (III), respectively. Although Fe (II) is more abundant under anoxic settings, iron is easily oxidized from Fe (II) to Fe (III) in an oxygen-containing environment. It results in the creation of iron oxides: ferrous oxide, FeO; ferric oxide, Fe_2O_3; and Fe_3O_4, which contains iron in both +2 and +3 oxidation states. The color of these oxides varies depending on their stage, with ferrous oxide being a black powder and ferric oxide being a reddish powder that occurs naturally as the mineral hematite [50]. In addition, Fe exhibits distinctive peaks in XPS spectrum that correspond to their different oxidation states. The FeO (Fe (II)) peak is generally detected at roughly 709 eV and 711 eV for Fe_2O_3 (Fe (III)) [51].

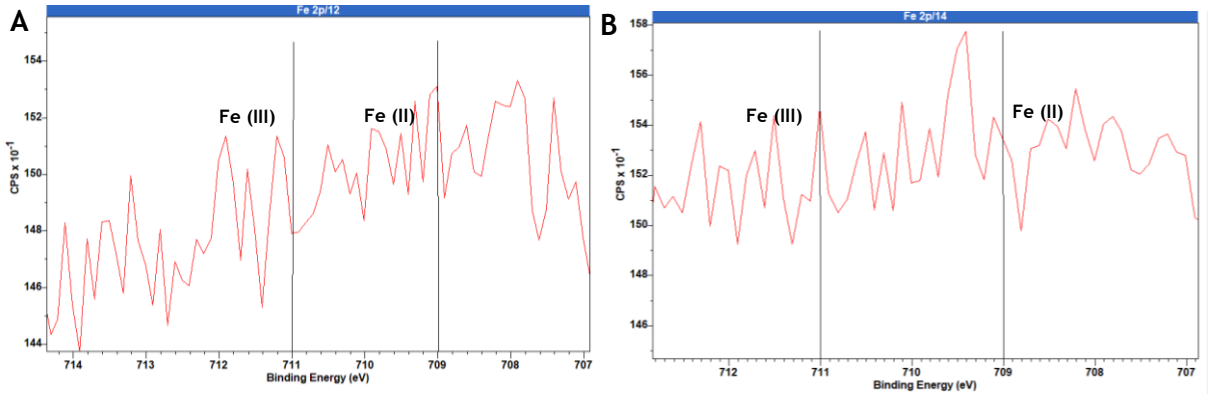

Figure 24- Fe's XPS spectrum for A) Bp1200 and B) Bp1300.

Figure 24 represents the zone of interest, so it shows XPS spectrum of Fe for the samples HAp1200 and HAp1300. Upon observing it, it is noticeable that as the sintering

temperature increases, there is an increase in the intensity of the peak corresponding to Fe (III) at around 711 eV. Conversely, the intensity of the Fe (II) peak at 709 eV decreases. As was mentioned earlier, the increase of the sintering temperature promotes the granules' transformation from white to grey/pink color.

Thus, HAp1200 sample exhibits a more grayish coloration, coinciding with a higher intensity of the peak corresponding to Fe (II), which is known for its black color. This suggests the formation of this oxide in the sample. In contrast, the sample sintered at 1300 °C shows a higher intensity of the peak at 711 eV, corresponding to Fe_2O_3, providing the appearance of a pink or red color.

In order to confirm that the color change is caused by iron oxidation. the samples were subjected, once only, to sintering in an oxygen-free argon atmosphere. In this controlled environment, the samples retained their initial white color even after the sintering process. Consequently, it can be inferred that maybe iron is the primary factor responsible for the color transformation observed as the sintering temperatures increase, as oxidation of the iron species occurs.

4.1.2. Biphasic Granules

4.1.2.1. Bulk Density

As was previously mentioned, a substitute for using HAp-granules had to be developed, leading to the creation of biphasic granules that contain both HAp and ß-TCP. This is because subjecting them to high temperatures is crucial for achieving the desired density and strength, however, high temperatures further impair the degradation of HAp, making it more crystalline and therefore slower to degrade. Although it can also lead to the formation of a new phase known as TTCP, with a higher degradation rate. So, considering the functional properties of these biomaterials, it is vital to assess the granules' changes after being combined with ß-TCP, namely their density and porosity distribution. The relative density values for each batch, along with their global porosity, as calculated using equation 4 from 3.3.4., are provided in table 9.

By analyzing table 9, the density of these biphasic samples tends to increase as the sintering temperature rises, leading to the decrease in percentage of pores in the samples, as observed in the values presented. However, a larger number of tests would be necessary to obtain a larger sample size and thus draw statistically significant conclusions.

Table 9- Relative density values obtained for each batch, along with their corresponding global porosity.

Batch	Bp1000	Bp1100	Bp1200	Bp1300
Relative density	0.70 ± 0.002	0.83 ± 0,005	0.99 ± 0.006	1.09 ± 0,006
Global porosity (%)	77.89 ± 0.07	73.89 ± 0.15	68.58 ± 0.18	65.54 ± 0.19

According to literature HAp has a density of 3.16 and, below 1120 °C, ß-TCP remains stable with a density of 3.07 [52]. Assuming these theoretical values, the density for granules with the formulation stipulated (75%HAp/25%ß-TCP) should be 3.14.

Even though the bulk density obtained from all batches was approximately one-third of the expected values for complete densification, as indicated in table 9, it can be concluded that the sintering process used for these granules did not lead to a full densification, resulting in the formation of porous structures. Like in the HAp samples, this can be attributed to the burning of alginate, which leads to the formation of pores. In addition, generally, achieving densification of ß-TCP is challenging due to its low phase transformation temperature in α-TCP, which impedes high-temperature sintering. In fact, this phase transformation slows down the densification of ß-TCP and, on the other hand, induces microcracks in the sample due to material expansion caused by the density difference between the phases and the surrounding material [52].

In addition, these lower values were expected due to differences in the properties of the constituent materials, such as their sintering temperatures and diffusion rates, which make challenging to achieve significant levels of general densification. However, it is advantageous for bone substitutes to have pores within a specific size range that promotes rapid bone ingrowth into the material and enhances the overall process of bone regeneration.

4.1.2.2.X-Ray Diffraction

As was mentioned before, to achieve the correct percentage of each bioceramic powder required to attain the desired final ratio (75/25) of HAp and ß-TCP phases in the materials' structure following the heat treatment, a calibration curve provided by FLUIDINOVA was used. Thus, the granules were analyzed using X-Ray diffraction to confirm that they consisted of the intended phases and possessed the desired ratio.

Figure 25 represents the diffractograms of all biphasic batches. By examining them, it is possible to comprehend the evolution of the intensity of the characteristic peaks of each phase as a function of the sintering temperature. To begin, for all batches, the peaks with the highest intensities correlate to the phase that is more abundant (75%

HAp). From a crystallinity standpoint, it was possible to conclude that Bp1000, Bp1100, Bp1200 and Bp1300 have high crystallinity since their diffractograms show narrow characteristics peaks, namely the 2θ= 31.8° for HAp and 30.95°for ß-TCP (maximum intensity values for HAp and ß-TCP) [53].

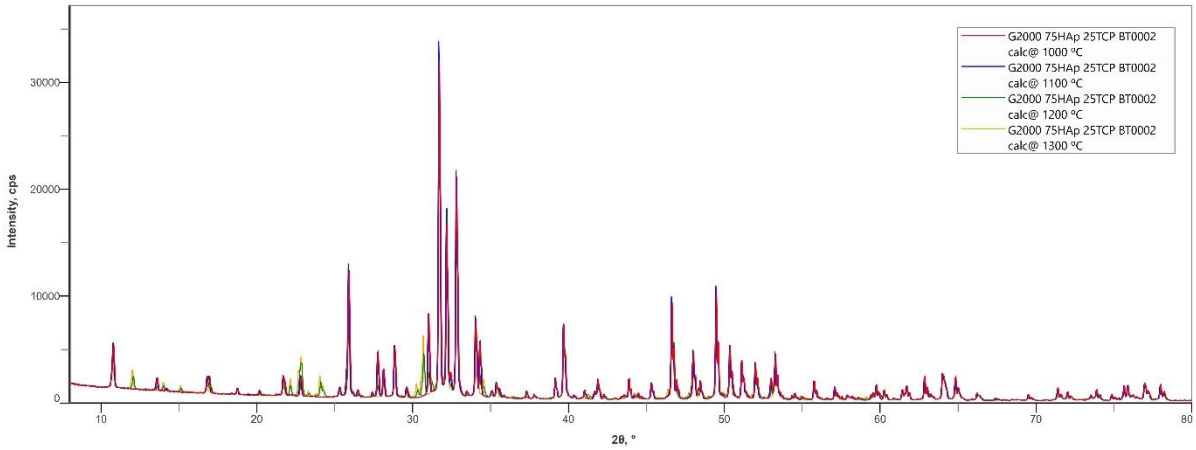

Figure 25- Diffractogram obtained through X-Ray diffraction analysis of all biphasic batches.

To conduct a more detailed comparison of the peak intensity evolution with sintering temperature, the diffractogram of the Bp1000 sample was superimposed with that of Bp1300 (figure 26). The diffractogram corresponding to the sample sintered at 1000 °C is represented by the red graph, while the one sintered at 1300°C is depicted in blue. Consequently, the phases present in each sample can be identified. As anticipated, the peaks corresponding to HAp are identified in both samples with higher intensity. However, as the temperature increases, the ß-TCP phase peaks are gradually replaced by α-TCP phase peaks, which indicates that the formation of this second new phase occurs.

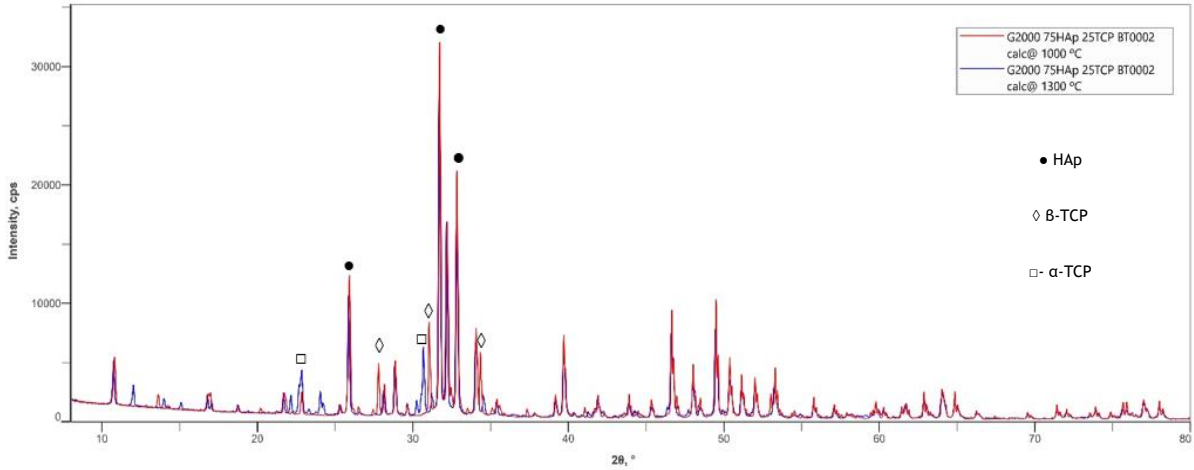

Figure 26- Diffractogram obtained through X-Ray diffraction analysis of Bp1000 and Bp1300.

To supplement the diffractograms presented earlier, table 10 present the real phase ratio of the batches. This table was designed with a permissible error margin of 5%, adhering to the guidelines set by ISO 13779-6. This tolerance allows for slight variations in the phase ratio while still maintaining an acceptable level of conformity.

Table 10- Batches' phase quantification obtained through XRD.

Batch	Bp1000	Bp1100	Bp1200	Bp1300
HAp (%)	78.83	78.39	78.56	76.43
β-TCP (%)	21.17	21.61	6.09	0
α-TCP (%)	0	0	15.35	23.57

By examining the phase ratio data provided in Table 10, it was determined that the desired composition of HAp and β-TCP in each batch was successfully achieved using the calibration curve. However, and as evidenced by the change in the peaks of each spectrum, it can be observed that with increasing sintering temperature, the β-TCP tends to undergo a transformation into α-TCP (Bp1200), until it is completely replaced by this new phase at 1300 °C.

Although β-TCP and α-TCP have the same chemical formula, they differ in crystal structure and solubility and β-TCP is more stable than α-TCP phase. Therefore, α-TCP is more reactive in aqueous systems, has a higher specific energy, and can be hydrolyzed to form a mixture of various calcium phosphates. Pure α-TCP has not received much interest in the biomedical field, mainly due to its rapid resorption rate. However, has been commercialized as a biphasic composite with HAp to produce bioresorbable porous ceramic scaffolds to be used as artificial bone grafts [54].

Therefore, since these two-phase granules had never been treated to such high temperature treatments in previous experiments, the development of α-TCP phase was an interesting novelty for both the study and the company in question. It is still necessary to assess the impact of this phase on the mechanical properties of the granules, which will be covered in the next chapters.

4.2. Mechanical Characterization

4.2.1. Monophasic Granules

4.2.1.1. Compressive tests

Given that the purpose of the granules is to be implanted in the human body, they will inevitably encounter different compressive forces exerted by the surrounding tissues.

Studies have demonstrated that the compressive strength of cortical bone is approximately between 100-200 MPa. On the other hand, the properties of trabecular or cancellous bone, since presents a porous structure, has lower compressive resistance, with values being reported between 10 and 80 MPa. The mechanical properties of cortical bone and trabecular bone can undergo significant alterations due to the person's age and diseases, where porosity is considered the primary physical property that contributes to

these changes. The porosity percentage of the material is crucial for bioceramics since it restricts the range of applications that a material can be used. Materials with high values of porosity cannot be used in sites where they are subject to high load values [55].

These two types of bone tissue have distinct levels of porosity: Cortical bone has a porosity of 5% to 15%, whereas the porosity of trabecular bone ranges from 40% to 95%. However, osteoporosis and diabetes can have profound consequences for individuals' quality of life, such as the deterioration of bone that causes an increase in porosity, and in turn the decrease in mechanical properties [56].

Therefore, it becomes crucial to investigate the HAp granules' mechanical response and behavior. The values obtained for the compression strength of each batch are illustrated in table 11.

According to SEM observations, the rise in sintering temperature led to the bonding of HAp crystals, resulting in reduced microporosity. Figure 27 shows that increasing the sintering temperature resulted in significantly higher compressive strength. Notably, at a sintering temperature of 1300 °C, pure HAp spherical granules exhibited superior mechanical strength compared to other temperatures. The statistical analysis done with four replicate per condition (n= 4) reveal that the compressive strengths are all significantly different ($p < 0.05$) and therefore we can state that HAp1300 has the highest strength with a significant difference compared to the others.

Table 11- Compressive strength's average values for each batch.

Batch	Compressive Strength (MPa)
HAp1000	2.03 ± 0.07
HAp1100	3.50 ± 0.05
HAp1200	7.50 ± 0.17
HAp1300	15.30 ± 0.72

However, the high porosity values observed in the granules can be attributed to insufficient sintering temperature, which did not effectively decrease the porosity between particles. This inadequacy resulted in weaker bonding between the particles of each granule, thereby compromising the compressive strength of the bioceramic material. Despite this, the strength measurements acquired fall within the typical range exhibited by trabecular bone (10-80 MPa), so we can infer that these granules have the potential to be used as substitutes for trabecular bone.

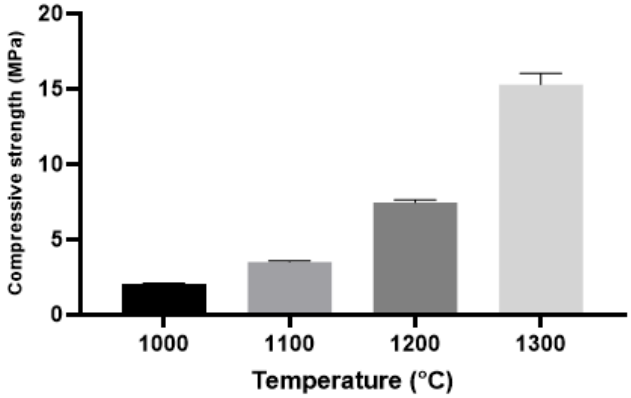

Figure 27- Compressive strength results obtained for each batch.

4.2.1.2. Vickers hardness tests

As it was mentioned before, several factors, including sintering temperature, porosity, sample stoichiometry, and trace elements present in the structure, have been demonstrated to affect the mechanical properties of HAp. Vickers hardness tests provide means to examine the connection between a material's structure and its mechanical properties at a microscopic level. Conducting hardness tests offers valuable insights into the mechanics of bone, contributing to a better understanding of its behavior [57]. Average hardness values of the sintered samples are given in Table 12.

The highest Vickers hardness value was observed in HAp1300, which means that with increasing sintering temperature there was an increase in the hardness values of the samples, and consequently in their mechanical strength. The statistical analysis done with four replicates (n=4) reveal that the hardness values are all significantly different ($p < 0.05$) and therefore we can state that HAp1300 has the highest mechanical strength with a significant difference compared to the others.

The graph depicted in Figure 28 demonstrates the impact of porosity, with their corresponding sintering temperature, on the hardness of the samples. It shows a reduction in hardness due to the increase in porosity, which is an expected result.

According to the literature, the tabulated microhardness value for non-porous HAp varies between 450 and 530 HV [55]. Despite the anticipated trend of increasing hardness with higher sintering temperatures, the obtained hardness values are consistent with the behavior of highly porous HAp, which typically exhibits reduced hardness compared to non-porous HAp. The presence of porosity directly impacts the mechanical strength of the material, resulting in decreased hardness.

Table 12- Average hardness values of each sample.

Batch	Vickers Hardness (average)
HAp1000	35 ± 4.43 HV 1
HAp1100	40 ± 3.27 HV 1
HAp1200	50 ± 3.81 HV 1
HAp1300	68 ± 13.61 HV 1

Furthermore, Vickers hardness values for highly porous HAp can vary considerably, depending on the extent of porosity and the specific structural characteristics of the sample. Considering that the studied HAp samples are inherently porous materials with inferior mechanical properties compared to dense materials, it is unsurprising that the observed hardness values and subsequent mechanical resistance values deviate significantly from the expected values. Nevertheless, as the compression tests conducted indicate, these values meet the requirements for applications involving trabecular bone replacement, where high porosity is crucial, allowing interaction with cells and growth factors, as well as bone tissue formation and remodeling.

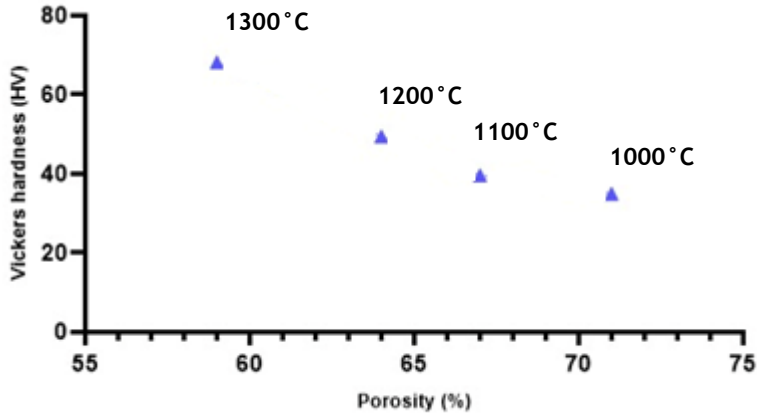

Figure 28- Vickers hardness of the samples as a function of their porosity.

To supplement and verify the Vickers hardness test, images of the indentations in both HAp1100 and HAp1300 samples (as shown in figure 29) were taken by using SEM. From these images and by measuring the visible diagonals it would be possible to calculate the hardness value of the samples and compare it with those obtained by the software.

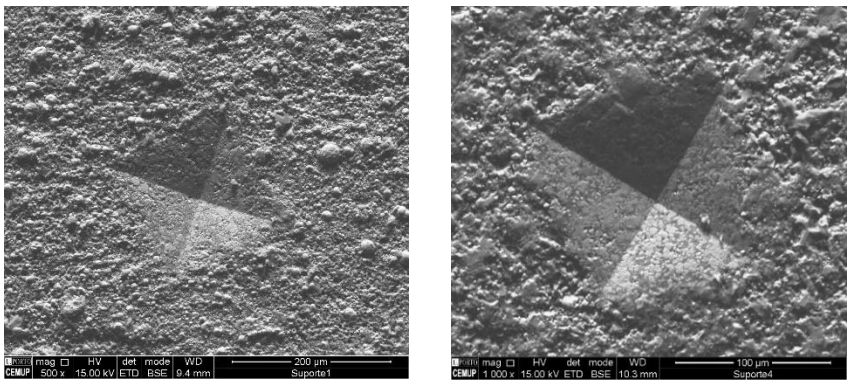

500 × **500 ×**

Figure 29- Indentations of Vickers hardness tests on: A) HAp1000 and B) HAp1300.

4.2.2. Biphasic Granules

4.2.2.1. Compressive tests

By analyzing table 13, compressive strengths ranged from 0.43 ± 0.18 MPa to 9.10 ± 3.12 MPa.

Table 13- Compressive strength's average values for each batch.

Batch	Compressive Strength (MPa)
Bp1000	0.43 ± 0.18
Bp1100	1.32 ± 0.33
Bp1200	3.43 ± 0.91
Bp1300	9.10 ± 3.12

Increased sintering temperature resulted in significantly increased compressive strength, as shown in figure 30. Notably, the biphasic spherical granules displayed greater mechanical strength at a sintering temperature of 1300 °C when compared to other temperatures. The statistical examination of the four samples' results (n=4) reveals that the compressive strengths are all considerably different ($p < 0.05$), and so

we can conclude that Bp1300 has the highest strength with a significant difference

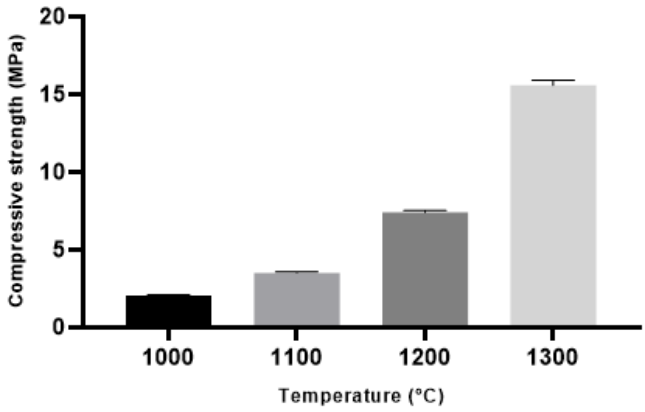

Figure 30- Compressive strength obtained values for each batch.

Although, the compressive strength of these scaffolds was significantly lower than that of cortical bone (100-200 MPa), but it closely matched that of cancellous bone (10-80 MPa). The lower values are directly associated to the high porosity levels, related to the sintering temperature not high enough to sinter the HAp completely, which consequently decrease its compressive strength. Thus, it is possible to conclude that HAp/β-TCP scaffolds are not suited for load-bearing applications, but they do display sufficient mechanical stability for bone regeneration/tissue engineering applications [55].

In summary, while these biphasic granules have lower compressive strength values compared to HAp ones, they still meet the requirements for final applications, mainly for trabecular bone substitution. Furthermore, they offer benefits such as improved solubility and the ability to achieve more stable phases, which are advantageous for this specific type of functions.

5. Conclusions and Future work

During this work, it was possible to successfully produce monophasic (HAp) and biphasic granules with a ratio of 75%HAp/25%ß-TCP, with different sintering temperatures (1000 °C, 1100 °C, 1200 °C and 1300 °C).

When the sintering temperature increased, the color of the HAp granules changed from white to pink. The ICP analysis revealed the presence of some elements at higher amounts than expected, namely iron. When heated to high temperatures, this element can create oxide compounds with a pink coloration. Consequently, an XPS study was done to identify this element's oxidation state, where were detected ferrous oxide (FeO) and ferric oxide (Fe_2O_3) and identified as potential causes for the color change.

The SEM analysis provided insights into the bonding between particles within the granules, which became more pronounced as the temperature increased. This phenomenon led to a decrease in porosity and an overall densification of the granules. Furthermore, XRD analysis indicated that at a sintering temperature of 1300 °C, HAp underwent a phase transformation to tetracalcium phosphate (TTCP), with 92.15% of HAp and 7.85% of TTCP, which can bring advantages from a degradation point of view. The mechanical properties were evaluated through compression tests and Vickers hardness tests. The values obtained varied with increasing sintering temperature (from 1000 °C to 1300 °C), ranging from 2.03 ± 0.07 MPa to 15.30 ± 0.72 MPa for compression strength and from 35 ± 4.43 HV1 to 68 ± 13.61 HV1 for Vickers hardness. These values fall within the expected range for highly porous materials suitable for trabecular bone replacement (10-80 MPa).

Subsequently, granules were produced with the formulation: 75%HAp/25% ß-TCP. Using XRD analysis it was possible to conclude that the ratios obtained were within the limits established and previously obtained by FLUIDINOVA. In addition, it was showed a phase transformation of ß-TCP into α-TCP, a phase with a high resorption rate, at 1300°C. In terms of mechanical properties, the compressive strength of biphasic granules was found to be lower than that of monophasic granules. This difference can be attributed to the higher porosity observed in the biphasic granules compared to the others.

Based on the findings, it can be inferred that the biphasic granules exhibited satisfactory mechanical performance as substitutes for trabecular bone (10-80 MPa). The higher porosity promotes rapid bone ingrowth into the material, which facilitates the integration of new bone tissue and enhances the overall process of bone regeneration. In addition, these granules have higher solubility and faster resorption.

In future work, there is a need for more comprehensive investigation into the observed color change. Specifically, the possibility of conducting the sintering process in an oxygen-free argon atmosphere should be explored. This approach may help prevent the occurrence of color alteration and provide a deeper understanding of the underlying mechanisms involved.

6. References

[1] D. C. Lobb, B. R. DeGeorge, and A. B. Chhabra, “Bone Graft Substitutes: Current Concepts and Future Expectations,” *Journal of Hand Surgery*, vol. 44, no. 6. W.B. Saunders, pp. 497-505.e2, Jun. 01, 2019. doi: 10.1016/j.jhsa.2018.10.032.

[2] A. R. Amini, C. T. Laurencin, and S. P. Nukavarapu, “Bone Tissue Engineering: Recent Advances and Challenges,” 2012.

[3] M. Canillas, P. Pena, A. H. De Aza, and M. A. Rodríguez, “Calcium phosphates for biomedical applications,” *Boletin de la Sociedad Espanola de Ceramica y Vidrio*, vol. 56, no. 3. Sociedad Espanola de Ceramica y Vidrio, pp. 91–112, May 01, 2017. doi: 10.1016/j.bsecv.2017.05.001.

[4] S. V. Dorozhkin, “Calcium orthophosphate-based bioceramics,” *Materials*, vol. 6, no. 9. MDPI AG, pp. 3840–3942, 2013. doi: 10.3390/ma6093840.

[5] W. Habraken, P. Habibovic, M. Epple, and M. Bohner, “Calcium phosphates in biomedical applications: Materials for the future?,” *Materials Today*, vol. 19, no. 2. Elsevier B.V., pp. 69–87, Mar. 01, 2016. doi: 10.1016/j.mattod.2015.10.008.

[6] R. Florencio-Silva, G. R. D. S. Sasso, E. Sasso-Cerri, M. J. Simões, and P. S. Cerri, “Biology of Bone Tissue: Structure, Function, and Factors That Influence Bone Cells,” *BioMed Research International*, vol. 2015. Hindawi Publishing Corporation, 2015. doi: 10.1155/2015/421746.

[7] J. S. Khurana, *Bone pathology*. Humana Press, 2009. doi: 10.1007/978-1-59745-347-9.

[8] Biga,L.; Dawson, S.; Harwell, A.; Hopkins, R; Kaufmann, J.; Lemaster, M.; (2019). BONE TISSUE AND THE SKELETAL SYSTEM. In *Anatomy & Physiology* (p.265–327).

[9] J. A. Buckwalter, M. J. Glimcher, R. R. Cooper, and R. Recker, “Bone Biology,” 1995. [Online]. Available: www.jbjs.org

[10] S. M. Ott, “Cortical or Trabecular Bone: What’s the Difference?,” *American Journal of Nephrology*, vol. 47, no. 6. S. Karger AG, pp. 373–375, Jul. 01, 2018. doi: 10.1159/000489672.

[11] G. Ramaswamy, M. W. Bidez, and C. E. Misch, “Bone Response to Mechanical Loads,” in *Dental Implant Prosthetics*, Elsevier Inc., 2015, pp. 107–125. doi: 10.1016/B978-0-323-07845-0.00006-3.

[12] D. J. Hadjidakis and I. I. Androulakis, “Bone remodeling,” in *Annals of the New York Academy of Sciences*, Blackwell Publishing Inc., 2006, pp. 385–396. doi:

10.1196/annals.1365.035.

[13] C. Laurencin, Y. Khan, and S. F. El-Amin, “Bone graft substitutes,” *Expert Review of Medical Devices*, vol. 3, no. 1. pp. 49–57, Jan. 2006. doi: 10.1586/17434440.3.1.49.

[14] V. Kartsogiannis and K. W. Ng, “Cell lines and primary cell cultures in the study of bone cell biology,” *Molecular and Cellular Endocrinology*, vol. 228, no. 1–2. Elsevier Ireland Ltd, pp. 79–102, Dec. 30, 2004. doi: 10.1016/j.mce.2003.06.002.

[15] H. C. Pape, A. Evans, and P. Kobbe, “Autologous Bone Graft: Properties and Techniques.” [Online]. Available: www.jorthotrauma.com

[16] T. Boyce, J. Edwards, and N. Scarborough, “The Influence of Processing on Safety and Performance.”

[17] N. Ortega, D. J. Behonick, and Z. Werb, “Matrix remodeling during endochondral ossification,” *Trends in Cell Biology*, vol. 14, no. 2. Elsevier Ltd, pp. 86–93, 2004. doi: 10.1016/j.tcb.2003.12.003.

[18] V. Campana *et al.*, “Bone substitutes in orthopaedic surgery: from basic science to clinical practice,” *J Mater Sci Mater Med*, vol. 25, no. 10, pp. 2445–2461, Sep. 2014, doi: 10.1007/s10856-014-5240-2.

[19] M. P. Ginebra, M. Espanol, Y. Maazouz, V. Bergez, and D. Pastorino, “Bioceramics and bone healing,” *EFORT Open Rev*, vol. 3, no. 5, pp. 173–183, May 2018, doi: 10.1302/2058-5241.3.170056.

[20] V. A. Dubok, “BIOCERAMICS ▫ YESTERDAY, TODAY, TOMORROW,” 2000.

[21] M. Bohner, “Resorbable biomaterials as bone graft substitutes,” *Materials Today*, vol. 13, no. 1–2. pp. 24–30, Jan. 2010. doi: 10.1016/S1369-7021(10)70014-6.

[22] Z. Sheikh, C. Sima, and M. Glogauer, “Bone replacement materials and techniques used for achieving vertical alveolar bone augmentation,” *Materials*, vol. 8, no. 6, pp. 2953–2993, 2015, doi: 10.3390/ma8062953.

[23] T. V Thamaraiselvi and S. Rajeswari, “Biological Evaluation of Bioceramic Materials-A Review,” 2004. [Online]. Available: http://www.sbaoi.org

[24] F. Baino, G. Novajra, and C. Vitale-Brovarone, “Bioceramics and scaffolds: A winning combination for tissue engineering,” *Frontiers in Bioengineering and Biotechnology*, vol. 3. Frontiers Media S.A., 2015. doi: 10.3389/fbioe.2015.00202.

[25] V. V. C. Azevedo, S. A. Chaves,; D C Bezerra, and ; A C F M Costa, “Materiais

cerâmicos utilizados para implantes", [Online]. Available: www.dema.ufcg.edu.br/revista

[26] "Hydroxyapatite Synthesis Methodologies: An Overview". *International Journal of ChemTech Research*, no. 2, pp. 903–907, 2010.

[27] M. Vallet-Regí, "Ceramics for medical applications," *Journal of the Chemical Society, Dalton Transactions*, no. 2, pp. 97–108, 2001, doi: 10.1039/b007852m.

[28] A. Szcześ, L. Hołysz, and E. Chibowski, "Synthesis of hydroxyapatite for biomedical applications," *Advances in Colloid and Interface Science*, vol. 249. Elsevier B.V., pp. 321–330, Nov. 01, 2017. doi: 10.1016/j.cis.2017.04.007.

[29] H. S. Sohn and J. K. Oh, "Review of bone graft and bone substitutes with an emphasis on fracture surgeries," *Biomaterials Research*, vol. 23, no. 1. BioMed Central Ltd., Mar. 14, 2019. doi: 10.1186/s40824-019-0157-y.

[30] J. Jeong, J. H. Kim, J. H. Shim, N. S. Hwang, and C. Y. Heo, "Bioactive calcium phosphate materials and applications in bone regeneration," *Biomaterials Research*, vol. 23, no. 1. BioMed Central Ltd., Jan. 14, 2019. doi: 10.1186/s40824-018-0149-3.

[31] M. Yashima, A. Sakai, T. Kamiyama, and A. Hoshikawa, "Crystal structure analysis of β-tricalcium phosphate Ca 3(PO4)2 by neutron powder diffraction," *J Solid State Chem*, vol. 175, no. 2, pp. 272–277, 2003, doi: 10.1016/S0022-4596(03)00279-2.

[32] M. Bohner, B. L. G. Santoni, and N. Döbelin, "β-tricalcium phosphate for bone substitution: Synthesis and properties," *Acta Biomaterialia*, vol. 113. Acta Materialia Inc, pp. 23–41, Sep. 01, 2020. doi: 10.1016/j.actbio.2020.06.022.

[33] M. Ebrahimi, M. G. Botelho, and S. V. Dorozhkin, "Biphasic calcium phosphates bioceramics (HA/TCP): Concept, physicochemical properties and the impact of standardization of study protocols in biomaterials research," *Materials Science and Engineering C*, vol. 71. Elsevier Ltd, pp. 1293–1312, Feb. 01, 2017. doi: 10.1016/j.msec.2016.11.039.

[34] BONE GRAFTS AND SUBSTITUTES MARKET SIZE & SHARE ANALYSIS - GROWTH TRENDS & FORECASTS (2023 - 2028). (2023). Mordor Intelligence. https://www.mordorintelligence.com/industry-reports/bone-grafts-and-substitutes-market

[35] Allied Market Research, "Bone Grafts and Substitutes Market by Type (Allografts, Bone grafts substitutes, Cell based matrices), by Application (Spinal fusion, Trauma, Joint reconstruction, Dental bone grafting, Craniomaxillofacial), by End user (Hospitals, Specialty clinics, Others): Global Opportunity Analysis and Industry Forecast, 2021-2031." Feb. 26, 2023.

[36] Grand View Research, “Bone Grafts and Substitutes Market Size, Share & Trends Analysis Report By Material Type (Allograft, Synthetic), By Application (Craniomaxillofacial, Dental, Foot & Ankle, Joint Reconstruction), By Region, And Segment Forecasts, 2023 - 2030.” Feb. 26, 2022.

[37] “Technical data sheet nanoXIM•Granules”. FLUIDINOVA, S.A., 2021. (Accessed Ap.22, 2023)

[38] “Technical data sheet nanoXIM•HAp200” FLUIDINOVA, S.A., 2021. https://www.fluidinova.com/docs/nanoxim_hap200_tds.pdf (accessed Ap. 22, 2023).

[39] “Technical data sheet nanoXIM•TCP600” FLUIDINOVA, S.A, 2021. (Accessed Ap. 22, 2023)

[40] Moreira, J. (2022).” DEVELOPMENT OF BIPHASIC GRANULES USING THE NANOXIM PROCESS FOR BONE REGENERATION” [Dissertação de Mestrado]. FEUP.

[41] “Bulk density and tapped density of powders. (2019). In EUROPEAN PHARMACOPOEIA.”.

[42] V. Pejchal, G. Žagar, R. Charvet, C. Dénéréaz, and A. Mortensen, “Compression testing spherical particles for strength: Theory of the meridian crack test and implementation for microscopic, fused quartz,” *J Mech Phys Solids*, vol. 99, pp. 70–92, Feb. 2017, doi: 10.1016/j.jmps.2016.11.009.

[43] I. S. Neira *et al.*, “An effective morphology control of hydroxyapatite crystals via hydrothermal synthesis,” *Cryst Growth Des*, vol. 9, no. 1, pp. 466–474, Jan. 2009, doi: 10.1021/cg800738a.

[44] C. C. Coelho *et al.*, “The antibacterial and angiogenic effect of magnesium oxide in a hydroxyapatite bone substitute,” *Sci Rep*, vol. 10, no. 1, Dec. 2020, doi: 10.1038/s41598-020-76063-9.

[45] A. Chetty, I. Wepener, M. K. Marei, Y. El Kamary, and R. M. Moussa, “HYDROXYAPATITE: SYNTHESIS, PROPERTIES, AND APPLICATIONS.”

[46] S. Ramesh, C. Y. Tan, S. B. Bhaduri, W. D. Teng, and I. Sopyan, “Densification behaviour of nanocrystalline hydroxyapatite bioceramics,” *J Mater Process Technol*, vol. 206, no. 1–3, pp. 221–230, Sep. 2008, doi: 10.1016/j.jmatprotec.2007.12.027.

[47] S. V. Dorozhkin, “Calcium orthophosphates in nature, biology and medicine,” *Materials*, vol. 2, no. 2. MDPI AG, pp. 399–498, 2009. doi: 10.3390/ma2020399.

[48] R. Chaim, M. Levin, A. Shlayer, and C. Estournes, “Sintering and densification of

nanocrystalline ceramic oxide powders: A review," *Advances in Applied Ceramics*, vol. 107, no. 3. pp. 159–169, Jun. 2008. doi: 10.1179/174367508X297812.

[49] Swain, S. (2009). Processing of Porous Hydroxyapatite Scaffold [Dissertação de Mestrado]. Ceramic Engineering National Institute of Technology Rourkela.

[50] M. Ilbert and V. Bonnefoy, "Insight into the evolution of the iron oxidation pathways," *Biochimica et Biophysica Acta - Bioenergetics*, vol. 1827, no. 2. pp. 161–175, Feb. 2013. doi: 10.1016/j.bbabio.2012.10.001.

[51] NIST X-ray Photoelectron Spectroscopy (XPS) Database Main Search Menu. (s.d.). National Institute of Standards and Technology. https://srdata.nist.gov/xps/main_search_menu.aspx

[52] M. Descamps, J. C. Hornez, and A. Leriche, "Effects of powder stoichiometry on the sintering of β-tricalcium phosphate," *J Eur Ceram Soc*, vol. 27, no. 6, pp. 2401–2406, 2007, doi: 10.1016/j.jeurceramsoc.2006.09.005.

[53] D. S. M. Etsger, M. R. Riege R, and D. W. Forem An, "Mechanical properties of sintered hydroxyapatite and tricalcium phosphate ceramic," 1999.

[54] S. V. Dorozhkin, "Calcium orthophosphates in nature, biology and medicine," *Materials*, vol. 2, no. 2. MDPI AG, pp. 399–498, 2009. doi: 10.3390/ma2020399.

[55] L. A. Cyster *et al.*, "The influence of dispersant concentration on the pore morphology of hydroxyapatite ceramics for bone tissue engineering," *Biomaterials*, vol. 26, no. 7, pp. 697–702, Mar. 2005, doi: 10.1016/j.biomaterials.2004.03.017.

[56] A. M. Yousefi, "A review of calcium phosphate cements and acrylic bone cements as injectable materials for bone repair and implant fixation," *Journal of Applied Biomaterials and Functional Materials*, vol. 17, no. 4. SAGE Publications Ltd, Oct. 01, 2019. doi: 10.1177/2280800019872594.

[57] S. M. Toker, A. Tezcaner, and Z. Evis, "Microstructure, microhardness, and biocompatibility characteristics of yttrium hydroxyapatite doped with fluoride," *J Biomed Mater Res B Appl Biomater*, vol. 96 B, no. 2, pp. 207–217, Feb. 2011, doi: 10.1002/jbm.b.31754.

Appendix I

Table 14- ICP analysis' results of the raw materials, the HAp powder and the granules produced.

	Semi-quantitative analysis								
	Element concentration (ppm)								
	Raw materials			Powder Hap	Granules				
Element	KH_2PO_4	$CaCl_2$	KOH	IM24SD01	1100-12	1100-12-t	1200-4-t	1250-4-t	1300-12-t
Ag	ND	ND	ND	ND	ND	ND	ND	ND	ND
Al	ND	ND	ND	ND	ND	ND	ND	ND	ND
As	ND	ND	ND	ND	ND	ND	ND	ND	ND
B	10	12	ND	26	27	27	26	27	29
Ba	ND	280	ND	100	106	101	101	103	108
Bi	ND	ND	ND	ND	ND	ND	ND	ND	ND
Ca	17	32 %	69	30 %	30 %	32 %	32 %	27 %	24 %
Cd	ND	ND	ND	ND	ND	ND	ND	ND	ND
Co	ND	ND	ND	ND	ND	ND	ND	ND	ND
Cr	ND	ND	ND	ND	ND	ND	ND	ND	ND
Cu	0,39	0,71	0,42	0,99	0,99	0,93	1,02	1,24	1,09
Fe	6,30	3,55	3,52	5,78	6,60	6,24	6,79	7,56	6,43
Hg	ND	ND	ND	ND	ND	ND	ND	ND	ND
K	14 %	5214	26 %	719	7	51	14	71	12
Li	ND	ND	ND	ND	ND	ND	ND	ND	ND
Mg	ND	10,1	-0,3	11,0	13,3	12,7	12,8	12,5	13,8
Mn	ND	ND	ND	ND	ND	ND	ND	ND	ND
Mo	ND	ND	ND	ND	ND	ND	ND	ND	ND
Na	30	2547	2037	174	104	212	140	135	189
Ni	ND	ND	ND	ND	ND	ND	ND	ND	ND
P	13 %	54	62	17 %	17 %	18 %	18 %	16 %	14 %
Pb	ND	ND	ND	ND	ND	ND	ND	ND	ND
Sb	ND	ND	ND	ND	ND	ND	ND	ND	ND
Se	ND	ND	ND	ND	ND	ND	ND	ND	ND
Si	2,4	1,4	1,5	36,8	43,7	42,3	41,9	42,0	45,3

Sn	ND	ND	ND	ND	ND	ND	ND	ND	ND
Sr	ND	86	ND	57	61	58	59	59	61
Ti	ND	ND	ND	ND	ND	ND	ND	ND	ND
Tl	ND	ND	ND	ND	ND	ND	ND	ND	ND
V	ND	ND	ND	ND	ND	ND	ND	ND	ND
W	ND	ND	ND	ND	ND	ND	ND	ND	ND
Zn	ND	ND	ND	ND	ND	ND	ND	ND	ND
Zr	ND	ND	ND	ND	ND	ND	ND	ND	ND
ND: non-detected									